



Department of Chemistry, University of Jyväskylä

DEVELOPMENT OF METHODS AND APPLICATIONS OF
LASER-INDUCED PLASMA SPECTROSCOPY IN VACUUM
ULTRAVIOLET

SAARA KASKI

Academic Dissertation
for the Degree of
Doctor of Philosophy

Jyväskylä, Finland 2005

Research Report No. 115

DEPARTMENT OF CHEMISTRY, UNIVERSITY OF JYVÄSKYLÄ
RESEARCH REPORT No. 115

**DEVELOPMENT OF METHODS AND APPLICATIONS OF
LASER-INDUCED PLASMA SPECTROSCOPY IN VACUUM
ULTRAVIOLET**

BY

SAARA KASKI

Academic Dissertation
for the degree of
Doctor of Philosophy

*To be presented, by permission of the Faculty of Mathematics and Science
of the University of Jyväskylä, for public examination in Auditorium FYS1,
on 21st December 2005, at 12 noon*



Copyright © 2005
University of Jyväskylä
Jyväskylä, Finland
ISBN 951-39-2374-6
ISSN 0357-346X

URN:ISBN:978-951-39-9875-2
ISBN 978-951-39-9875-2 (PDF)
ISSN 0357-346X

Jyväskylän yliopisto, 2023

PREFACE

The work presented in this thesis has been carried out in the years 2001 and 2005 at the Department of Chemistry, University of Jyväskylä. Financial support from Jenny and Antti Wihuri Foundation and a scholarship from University of Jyväskylä are gratefully acknowledged.

I would like to express my warmest gratitude to my supervisor Dr. Heikki Häkkänen. You introduced me to the world of laser-induced plasma spectroscopy, gave both technical and scientific support in lab and were a mighty opponent and referee, while I introduced new results and theories from the experimental measurements. In my opinion, we have made a great team, as regards to laser-induced plasma spectroscopy, teaching in the student laboratory, or carrying excimer lasers around.

I would also like to extend my gratitude to Prof. Jouko Korppi-Tommola for giving me opportunity to pursue the degree of Doctor of Philosophy and his sincere faith in my skills and his support during the process. I am also grateful to Prof. Henrik Kunttu for his encouragement while I was writing this thesis. Both professors have been of great assistance in finding the funding for my work, thank you for that.

I have spent most delightful moments at the work among you, dear colleagues at Department of Physical Chemistry, from the present and the past. I would like to express my warmest thanks; I will never forget the inspiring and ingenious discussions during the tea breaks, where in my opinion you really have demonstrated absolute creativeness. And thank you for participating the numerous excursions and artistic projects, it has been a pleasure! Also people from the whole Department of Chemistry have been of great assistance in many practical matters and problems, which I have encountered during these years. Thank you for your cooperation.

My sincerest appreciation goes to my family. Now I truly do understand, what lies behind, when people thank their family for the support and encouragement. I would also like to express my gratitude to my friends and relatives who have enabled me to have life outside the work, too.

Special thanks are reserved to my dear husband Sami. I wouldn't have achieved this much without you. Thank you for being there for me.

Jyväskylä, December 2005

Saara Kaski

ABSTRACT

A novel experimental setup for laser-induced plasma spectroscopy for the measurements in the vacuum ultraviolet (VUV) spectral region has been developed. The method is based on use of a purge gas to eliminate atmospheric absorption of VUV light emitted from plasma. A small Czerny-Turner spectrograph was purged with argon or nitrogen to prevent atmospheric absorption inside the spectrograph. The gas flow through the slit of the spectrograph purged the optical path between the slit and the plasma, which was generated near the spectrograph. Emission lines in the VUV region were detected down to 130 nm with an intensified charge-coupled device equipped with MgF₂ input window.

The setup for VUV analysis was used in two different applications. The potential of VUV detection in analysis of sulfide minerals was demonstrated with drill core samples. Main minerals at each sampling location were identified from their emission spectra in a fitting procedure, where a set of prerecorded reference spectra served as a data base. It was suggested, that the determined mineral distributions could be used to *in situ* sorting of the drill core samples in mines.

Feasibility of the VUV setup in analysis of chlorine and bromine from halogenated organic compounds was studied. In the purging arrangement strong atmospheric absorption at the wavelengths below 160 nm was observed and therefore a small sample chamber was used in these experiments. Carbon emission lines were used as an internal standard and linear correlation was found between the carbon and halogen emission intensity ratio and the corresponding atomic ratio of the compound. According to the results compounds containing 90 carbon atoms and one bromine atom could be detected in VUV. For chlorine compounds the respective ratio was only 20:1 due to the low transmission efficiency of the experimental setup.

In all measurements the plasma was generated with excimer lasers operating at UV wavelengths. Therefore influence of plasma shielding was also studied. It was observed, that at high irradiances ($>1 \text{ GW cm}^{-2}$) from ArF and KrF excimer lasers, emission intensities are significantly attenuated, also at longer delay times, as less energy of the laser pulse can reach the surface of the sample because of the plasma shielding. The influence of the laser repetition rate on shielding was found negligible. In argon atmosphere the attenuation was pronounced when compared to measurements in air, which may be caused by breakdown of argon gas in front of the sample.

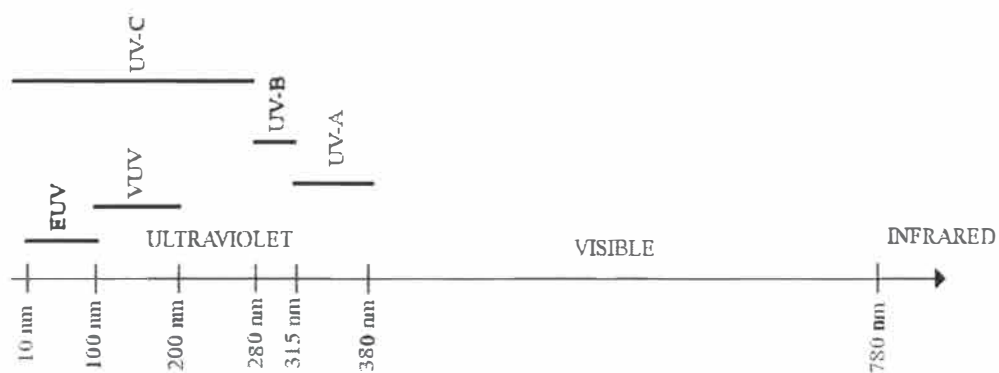
LIST OF ORIGINAL PUBLICATIONS

The main results of this thesis are presented in the following original research papers, which will be referred to in the text by their Roman numeral.

- I **Laser-Induced Plasma Spectroscopy to as Low as 130 nm When a Gas-Purged Spectrograph and ICCD Detection are Used**
Saara Kaski, Heikki Häkkänen, Jouko Korppi-Tommola
Applied Optics: Lasers, Photonics, and Environmental Optics **2003** 42 6036-6039.
[https://doi.org/ 10.1364/AO.42006036](https://doi.org/10.1364/AO.42006036)
- II **Sulfide mineral identification using laser-induced plasma spectroscopy**
Saara Kaski, Heikki Häkkänen, Jouko Korppi-Tommola
Minerals Engineering **2003** 16 1239-1243.
<https://doi.org/10.1016/j.mineng.2003.05.001>
- III **Determination of Cl/C and Br/C ratios in pure organic solids using laser-induced plasma spectroscopy in near vacuum ultraviolet**
Saara Kaski, Heikki Häkkänen, Jouko Korppi-Tommola
Journal of Analytical Atomic Spectrometry **2004** 19 474-478.
<https://doi.org/10.1039/B315410F>
- IV **A spectroscopic study of shielding in plasmas generated by excimer laser radiation**
Saara Kaski, Heikki Häkkänen, Jouko Korppi-Tommola
Analytical and Bionanalytical Chemistry, submitted.

ABBREVIATIONS

CCD	Charge-coupled Device
EUV	Extreme Ultraviolet
IB	Inverse Bremsstrahlung
ICCD	Intensified Charge-coupled Device
IR	Infrared
LIBS	Laser-induced Breakdown Spectroscopy
LIPS	Laser-induced Plasma Spectroscopy
LOD	Limit of Detection
LTE	Local Thermodynamic Equilibrium
LTSD	Lens-to-sample Distance
MPI	Multiphoton Ionization
NIR	Near Infrared
PDA	Photodiode Array
PMT	Photomultiplier Tube
UV	Ultraviolet
VUV	Vacuum Ultraviolet



Optical spectrum of the electromagnetic radiation. Wavelengths below ~ 10 nm are considered as soft X-rays. In the ultraviolet spectral range EUV, *i.e.*, extreme UV may also be written as XUV if also wavelengths below 10 nm are included. There may be some small variations of definitions of the regions depending on the reference.

TABLE OF CONTENTS

PREFACE	III
ABSTRACT	V
LIST OF ORIGINAL PUBLICATIONS	VII
ABBREVIATIONS	IX
TABLE OF CONTENTS	XI
1 INTRODUCTION	1
2 LASER-INDUCED PLASMA	3
2.1 GENERAL FEATURES OF LASER-INDUCED PLASMA	3
2.1.1 <i>Laser ablation</i>	3
2.1.2 <i>Plasma generation</i>	4
2.1.3 <i>Influence of the ambient gas</i>	6
2.2 PLASMA GENERATION WITH EXCIMER LASERS	8
2.2.1 <i>Excimer lasers</i>	8
2.2.2 <i>Focusing and ablation craters</i>	8
2.2.3 <i>Plasma temperature</i>	11
2.2.4 <i>Plasma shielding</i>	15
3 MEASUREMENTS IN VACUUM ULTRAVIOLET	19
3.1 PREVENTING ATMOSPHERIC ABSORPTION IN LIPS ANALYSIS	19
3.2 DETECTION OF THE PLASMA EMISSION IN VACUUM ULTRAVIOLET	23
3.2.1 <i>Spectrographs</i>	24
3.2.2 <i>Detectors</i>	24
4 LIPS STUDIES IN VACUUM ULTRAVIOLET	27
4.1 SULFIDE MINERALS	27
4.1.1 <i>LIPS in analysis of geological samples</i>	27
4.1.2 <i>Analysis of drill core samples in VUV</i>	28
4.2 CHLORINATED AND BROMINATED ORGANIC COMPOUNDS	32
4.2.1 <i>LIPS in analysis of chlorine and bromine</i>	32
4.2.2 <i>Analysis of solid organic compounds</i>	32
5 SUMMARY	37
REFERENCES	39

1 INTRODUCTION

Laser-induced plasma spectroscopy (LIPS), also known as laser-induced breakdown spectroscopy (LIBS), is an analytical technique based on direct spectral information of the plasma produced in laser ablation process. LIPS analysis can be performed from samples in gaseous, liquid or solid state, because with high laser irradiances, plasma can be generated from any sample. The main advantages of LIPS are its capability of rapid, simultaneous multielemental analysis and a possibility to perform direct analysis from solid samples with minimal sample preparation. The method allows also determination of spatial distributions of inhomogeneous materials and analysis of depth profiles of coatings. The technique is well established in analysis of various materials, which can be noted from several reviews,¹⁻⁷ but LIPS analysis is still under development and new applications and technical innovations are introduced especially for on-line analysis.⁸⁻²²

The emission spectrum is characteristic for each emitting element in the plasma which allows reliable identification of the elements. The characteristic emission intensity is proportional to the content of the element in the sample, which allows quantitative analysis, provided that proper calibration samples are available. The spectrum contains numerous emission lines from the atomic and ionic transitions of the sample, which on the one hand is advantageous, when qualitative information on the sample is needed, but on the other hand may lead to spectral interferences. The interferences may be avoided if a spectral region free of overlapping lines can be used. If the concentration of the element of interest is low, an intensive characteristic emission line with least interference from overlapping lines has to be selected. The wider the spectral range available, the more versatile emission spectroscopy is for analysis.

Most of the LIPS analyses reported so far have been carried out in the wavelength region between 200 nm and 800 nm. However, several elements

with non-metallic character (for example S, Br, I, P, C, As, Cl) have intensive emission lines in the vacuum ultraviolet (VUV) region, *i.e.*, below 200 nm. For example, the strongest lines of chlorine are located between 130 nm and 140 nm. Detection in the VUV range allows analysis of some elements at lower concentrations than is possible in the UV or in the visible spectral regions. Spectral interference in the VUV may be smaller or negligible in complicated sample matrices, because certain elements (like Fe, Ni) containing high density of emission lines in the near-UV or in the visible, have fewer and/or less intensive emission lines in the VUV. These advantages make VUV an interesting spectral region for LIPS analysis, but only a few groups have so far worked in this region. One reason may be that the detection of atomic emission in the VUV becomes difficult with ordinary LIPS equipment because of atmospheric absorption.

In this thesis conventional Czerny-Turner spectrograph and intensified charge-coupled device were used in near VUV as low as 130 nm by eliminating the atmospheric absorption with a purge gas. It was demonstrated, that especially for detection of sulfur in VUV only a simple setup is needed. The experimental setup was applied to analysis of chlorinated and brominated organic samples and sulfide minerals. Because throughout the study excimer lasers operating at UV wavelengths were used, their plasma generation and shielding was also studied.

2 LASER-INDUCED PLASMA

2.1 General features of laser-induced plasma

Interaction of highly energetic, pulsed laser light with material leads to explosion and a formation of plasma. The following description of ablation process and plasma generation is restricted to lasers having pulse durations of the order of nanoseconds, because they were used in the study.

2.1.1 Laser ablation

At the sample surface part of the laser radiation is reflected and part is absorbed, depending on the optical properties of the material and the laser wavelength. The absorptivity in most materials is higher at short than long wavelengths. The penetration depth of the radiation for instance in metals is typically some tens of Ångströms.²³ In the focal region the optical energy is instantaneously converted to heat and vaporization at the surface begins. At high irradiances also the layers below the surface reach their boiling temperature due to thermal conduction in the material. The temperature in the layers below becomes soon higher than at the surface because of the cooling vaporization at the surface of the material. This leads to increased pressure in the sublayers and finally to explosion, *i.e.*, laser ablation.^{23,24}

2.1.2 Plasma generation

Right after the ablation the material vapor is partly ionized due to thermal or multi-photon ionization (MPI), the mechanism depending on the irradiation wavelength. In the NIR and at longer wavelengths, the electron density increases in the vapor mainly due to inverse bremsstrahlung (IB), first due to collisions between the electrons and neutrals and later between electrons and charged particles. At UV wavelengths the electron density growth is dominated by photoionization processes, which is also seen at low pressures, where the collision frequency is low.^{1,23} For example, the energy of one ArF laser photon at 193 nm (~6.4 eV) exceeds the first ionization potential of all alkaline metals, but for Nd:YAG laser operating at 1064 nm (~1.2 eV) several photons are required for photoionization of even the alkaline metals. In both cases also the thermal ionization produces charged species during the laser irradiation. The absorption of the laser pulse to the ablated material via IB and MPI and the resulting temperature increase are typically so rapid processes, that only near the threshold irradiances significant expansion of the hot material vapor occurs before the formation of the ionized plasma plume.²⁵

Threshold irradiances to initiate plasma depend on the material and are typically 10^8 - 10^9 W cm⁻², although irradiances as low as 10^6 W cm⁻² have been successful in solid samples.²³ For example, an ArF excimer laser pulse having a duration of 8 ns and energy of 1 mJ gives irradiance of $\sim 10^9$ W cm⁻² if the spot diameter is 125 μ m.

The plasma contains free atoms, electrons, ions, molecules, small solid particles, liquid droplets and clusters from the ablation process.²⁶ When the hot, high-pressured and luminous plasma expands to the surrounding atmosphere, it generates a shock wave and an acoustic pulse. The expansion velocity depends on the ambient pressure and *e.g.* for KrF laser initiated plasma average plume velocities of 2000 – 8000 m/s have been measured at laser irradiances from 0.08 to 0.4 GW cm⁻².²⁷ The luminosity is caused mainly by the plasma from the ablated material, but to some extent also by the shock-heated plasma from the ambient gas particles.²⁸

The energy of the laser pulse is coupled to the propagating plasma, but also direct heating and ablation of the sample material continues in the early stages of the plasma evolution. Vapor particles and droplets can cause scattering of laser radiation. Pulse energy is transferred to electrons in the plasma by IB processes, thus increasing the plasma temperature and electron density. Because IB is highly dependent on the electron concentration in the plasma, its importance can increase during the ablation, when MPI serves as a seeding mechanism. In case of very high laser irradiances, the plasma oscillation frequency due to the high electron density may exceed the frequency corresponding to the laser wavelength and the plasma core can become opaque to the laser radiation. Heating of the sample can in this case continue only indirectly by thermal radiation from the plasma plume. Also the heated ambient gas in the path of the laser beam can absorb the energy of the laser pulse.²⁵

The energy density in the plasma is extremely high, which promotes the expansion to the surroundings for a long time after laser pulse.²⁸ The energy of the plasma is transferred to the surrounding atmosphere with combination of several mechanisms, *e.g.* heating caused by the shock wave, radiative transfer and thermal conduction.^{1,25} The size of the bright core of the plasma decreases with time, as expansion to the surroundings proceeds and cools the plasma.²⁹ The temporal behavior of the laser-induced plasma depends mainly on the sample material, laser irradiance, ambient gas composition and pressure. Lifetime of the plasma can vary from ~ 300 ns to more than $40 \mu\text{s}$.²⁸ In liquids the time-scales are typically shorter than in solid or gaseous samples.¹ At early stages of the plasma evolution the spectrum is dominated by intense continuum caused by the Bremsstrahlung and recombination of ions and electrons. At later detection times ionic and atomic emission lines can be observed. The temporal behavior of the emission lines is dependent on the sample matrix (see Fig 1).

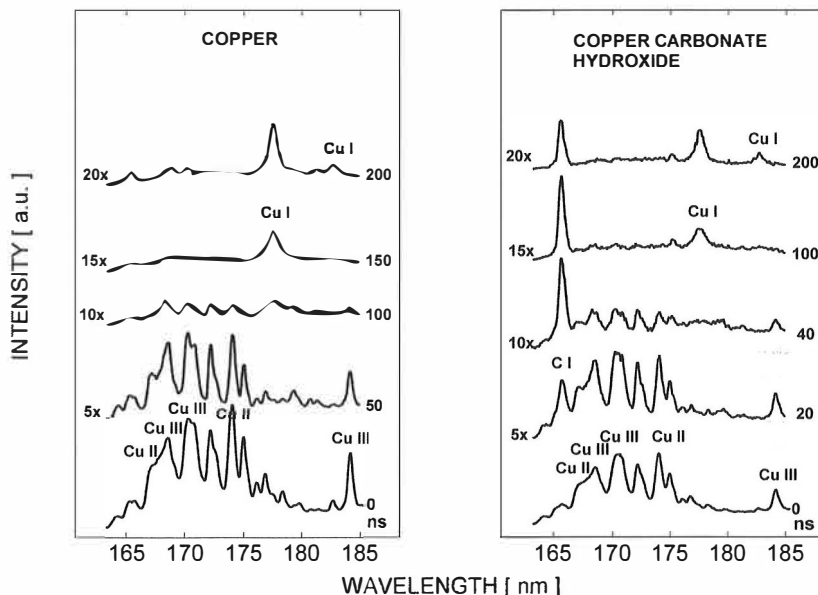


FIGURE 1: Spectra of metallic copper and copper carbonate hydroxide measured in the VUV spectral region as a function of the delay time *i.e.* time between the laser pulse and the detection. The pulse energy of the ArF laser was 1 mJ and the spot size $\sim 1 \times 10^{-4} \text{ cm}^2$. The spectra at longer delay times are magnified in intensity for better comparison.

When the expanding plasma cools, also new molecules composed of the atoms of the plasma and the ambient gas may be formed. For example, in laser-induced plasmas ablated in air from carbon-rich materials CN emission bands can be observed (Fig. 2). For the spectroscopic analysis the suitable region in time and space has to be determined for each sample type separately, because the decay times of different emission lines in the plasma can vary significantly.

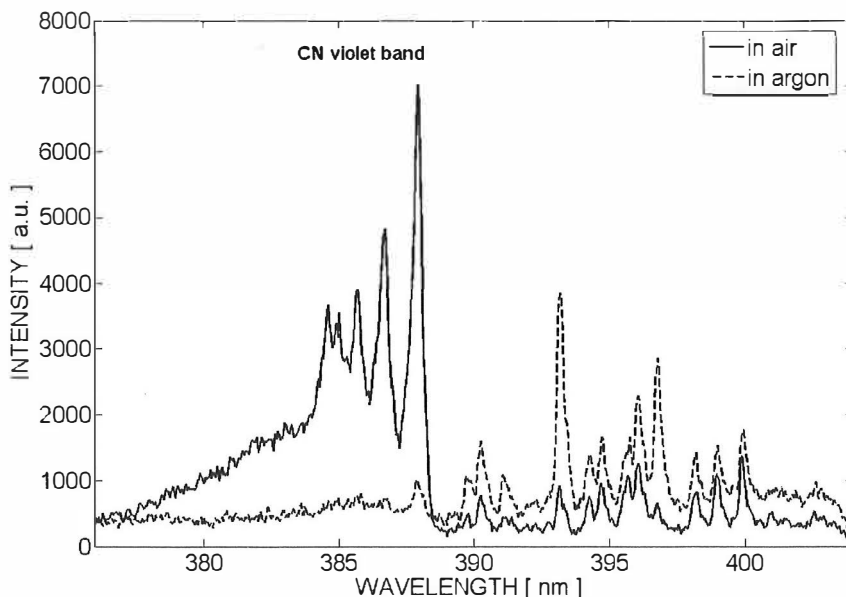


FIGURE 2: Emission lines of CN violet band $B^2\Sigma^+ \rightarrow X^2\Sigma^+$ from blue print ink sample containing nitrogen, measured in air (solid) and in argon (dash line) with 10 pulses from ArF excimer laser. The delay time was 100 ns and the gate width was 500 ns.

2.1.3 Influence of the ambient gas

In ablation of solids, noble gases may be chosen for the ambient gas instead of air, because noble gas atoms slow down the expansion and thus cooling of the plasma, when compared to air. Therefore higher emission intensities can be obtained at spectroscopic measurements in noble gas atmosphere. The decay of the emission line intensities is slower in argon atmosphere as shown in Fig. 3. The ambient gas is also ionized and excited, which in the ablation process may serve as a reservoir of the laser energy. On the other hand, the inverse bremsstrahlung has been observed to be most effective in argon,³⁰ which can increase plasma shielding. Almost two times higher emission intensities have been observed in argon under same experimental parameters than in air.³¹ However, the increase of the intensity level is pronounced at longer delay times (see Fig. 3).

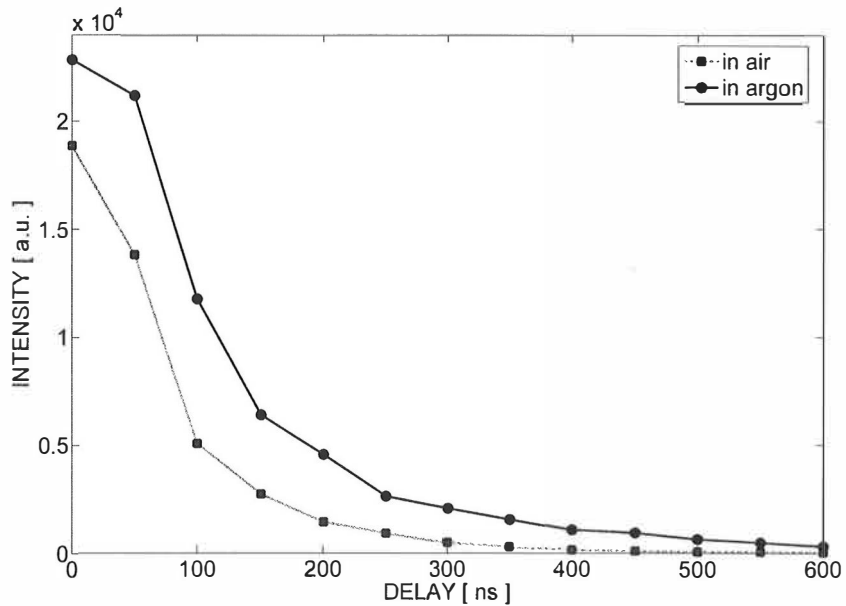


FIGURE 3: Emission intensity of the 288.1 nm background corrected silicon emission line measured from a glass sample in air (black) and in argon (gray) with 5 pulses from ArF excimer laser at 0.5 mJ pulse energy. The delay time was 100 ns and the gate width was 50 ns.

Emission of laser-induced plasma in various pressures has been mostly studied in air, argon, helium and nitrogen. It has been observed, that maximum intensity can be obtained in argon at reduced pressure. For example, in plasma generated by a XeCl excimer laser the maximum intensity was obtained at a pressure of ~ 70 mbar,³² while for a Nd:YAG laser a pressure of ~ 140 mbar has been found optimal.³³ The optimal pressure regarding the maximum intensity obtained from the measurement may depend somewhat on the laser wavelength, but most likely on the different laser pulse energies used.

At very low ambient pressures the plasma energy losses are higher due to the almost free expansion to the surroundings and the emission lines may become weaker. Simultaneously the plasma shielding is less severe in the laser beam path and thus the amount of ablated mass and the emission intensity can increase at reduced pressure.³⁴

2.2 Plasma generation with excimer lasers

In addition to the plasma formation mechanisms described in chapter 2.1.2 the laser wavelength affects to the ablation efficiency. Absorption coefficients of materials are wavelength dependent; typically the shorter the wavelength the higher the absorbance of the material. Thus, with an excimer laser operating at UV wavelengths, in principle, more material could be ablated per pulse. Such behavior has also been observed in the measurements of mass ablation rates in solid samples.^{29,35}

2.2.1 Excimer lasers

Excimer lasers are gas lasers, which contain rare-gas halide molecules, *i.e.*, diatomic molecules composed of a rare-gas atom and a halogen atom, for example argon and fluoride. The electronically excited state of such diatomic molecule is a tightly bound exciplex, but the ground state of the molecule is dissociative, leading to population inversion between the states. Transition from the excited state to the ground state produces a UV photon at a characteristic wavelength of the excited complex. Short wavelengths of the excimer lasers offer high excitation energies and very efficient multiphoton ionization.

The excimer laser gas mixture consists of ~0.1% - 0.5% of halogen, ~5% - 10% of rare gas and the buffer gas, which is helium or neon, at total pressures from 1.5×10^5 Pa to 6×10^5 Pa. High purity of the laser gases is important for efficient lasing, as halide ions are very reactive. The lifetime of the excimer gas mixture is typically limited to $\sim 10^7$ laser pulses because of chemical reactions between the gas and the chamber walls. A high-voltage electric discharge is applied to ionize the gas. Peak voltage can be up to 50 kV and peak current ~ 100 kA with a current rise times of 30 ns to 40 ns. Buffer gas is required to absorb part of the kinetic energy when the excimer is formed, otherwise the molecule would not remain in the bound state. The number of excited molecules leading to laser action is typically 10^{14} cm^{-3} to 10^{15} cm^{-3} .³⁶

2.2.2 Focusing and ablation craters

Since the radius of the focal cross section of a laser beam is directly proportional to wavelength of the laser,²⁶ UV wavelengths offer smaller spot sizes and better spatial resolution than visible or NIR lasers. In this thesis ArF and KrF excimer lasers, operating at 193 nm and 248 nm, respectively, were used to generate laser-induced plasma. The pulse duration of the ArF laser was 8 ns and that of the KrF laser 9 ns. The beam profile in most excimer lasers is rectangular, having a flat top spatial profile in the longer cross profile dimension, and more or less near-Gaussian at the shorter dimension.³⁷ For example, the beam size of ArF laser is 4×7 mm and the divergence is $\sim 1 \times 2$ mrad, but the divergence can be even larger in excimer lasers.

Tightness of focusing of the ArF excimer laser with a 40-mm focal length planoconvex lens was studied by inspection of ablation craters in printed and coated paper, using three aperture sizes from 1 to 3 mm (see Fig. 4). In the craters ablated near the focal point, the influence of diffraction and divergence of the excimer laser beam can be observed. Crater shapes vary depending on the position of the focal point with respect to the sample surface. In principle the plano-convex lens has low spherical aberration, but the influence of this effect can be observed in craters at negative LTSD values, *i.e.*, when the laser beam is focused inside the sample. The bottom of the crater is not flat, which is most likely caused by the difference in focal lengths of the incoming rays near and far from the optical axis (see Fig. 5), resulting in varying irradiances at the sample surface. The best ablation craters were obtained, when the LTSD value was positive, *i.e.*, the focal point was in front of the sample.

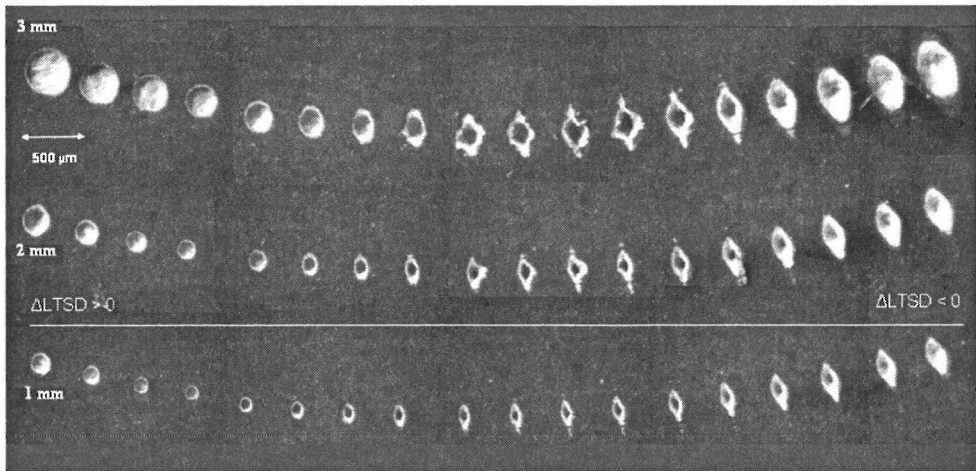


FIGURE 4: Ablation craters created with 100 pulses from an ArF laser on printed, coated paper with a 40-mm lens. Positive and negative values of lens-to-sample distance indicate that the focal point is in front of the sample and behind the sample surface, respectively. The laser energy was set to 4.0 mJ and with an aperture diameter of 3 mm energy of 1.5 mJ was selected. With diameter of 2 mm and 1 mm the respective energies were 0.5 mJ and 0.25 mJ.

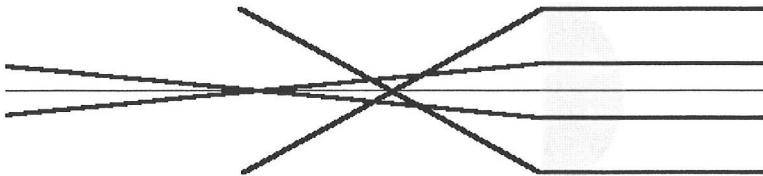


FIGURE 5: Spherical aberration in a planoconvex lens for rays near and far from the optical axis.³⁶

The spot sizes for the three apertures as a function of LTSD are presented in Fig. 6. For excimer lasers the spot size is typically limited more by divergence than diffraction (see Fig. 7), because the incident rays are not parallel. Difference in the depth of focus caused by the spherical aberration can be observed in Fig. 6 from the relative LTSD values at the smallest spot size, *i.e.*, with the smallest aperture the effective focal length of the lens is longer than that of the largest aperture.

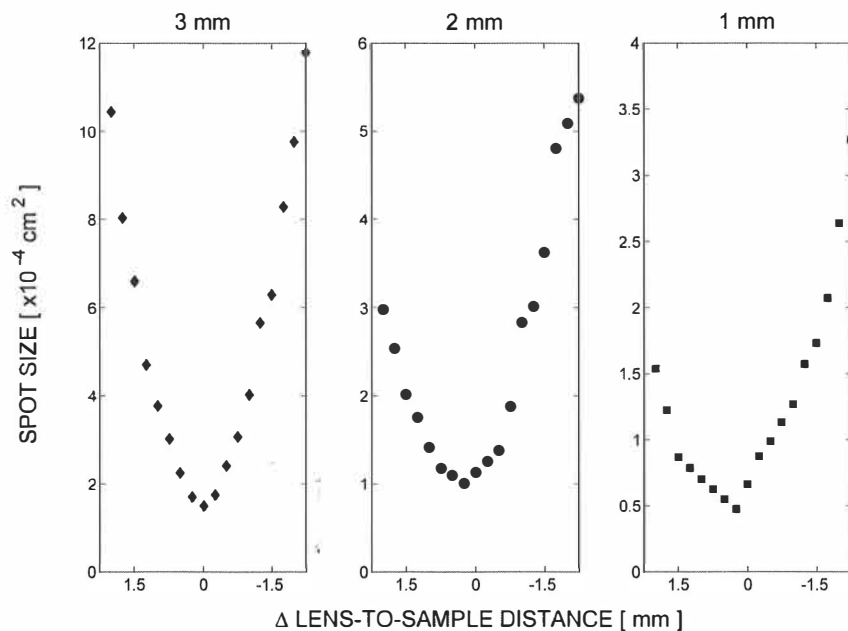


FIGURE 6: Spot sizes determined from the craters shown in Fig. 4 neglecting the ablation caused by diffraction. The error for the spot sizes was estimated to be of the order of $1 \times 10^{-5} \text{ cm}^2$.

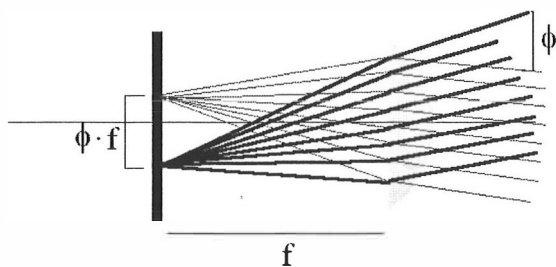


FIGURE 7: Spot size generated in a lens with a focal length of f and a beam divergence of ϕ .³⁶

With the excimer lasers nearly flat-top ablation craters have been obtained by selecting the central part from the beam with a circular aperture and by focusing the beam in front of the sample (see Fig. 8). However, the ablation rate depends on the laser pulse energy and the spot size. Also the sample material (*e.g.* hardness, thermal properties) has an effect on crater formation and shape.

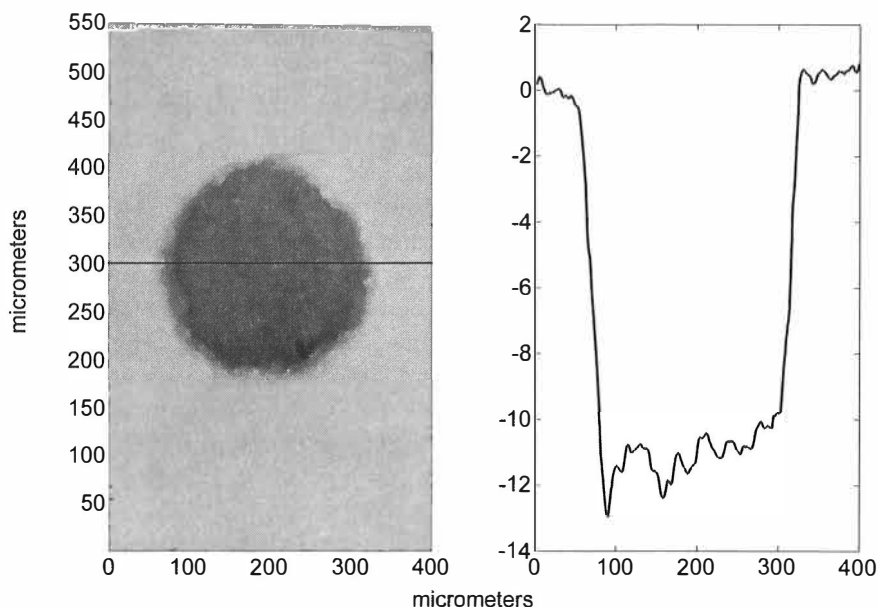


FIGURE 8: Ablation crater created by ArF laser on a coated paper. Microscope image and the depth profile were generated using a confocal profilometer. For ablation 20 pulses were used.

2.2.3 Plasma temperature

Plasma temperature is an important factor that contributes to dissociation, atomization, ionization and excitation processes in the plasma. In laser-induced plasma the electron density is typically of the order of $10^{15} - 10^{19} \text{ cm}^{-3}$ and the temperature is in range of $10^4 - 10^5 \text{ K}$.³⁸ The electron density in the plasma may be estimated from the Stark broadening of emission lines from isolated atoms or singly charged ions. In that case the effect of the Doppler broadening may be in many cases considered negligible compared to the broadening caused by the charged species. The emission lines should not suffer from the self-absorption³⁹, *i.e.*, the plasma should be optically thin for these lines. The plasma temperature is typically spectroscopically determined by using the Boltzmann plot method, in which the emission line intensity is related to the temperature T by Boltzmann distribution given in Equation 1.

$$\ln\left(\frac{I_{kl} \cdot \lambda}{g_k \cdot A_{kl}}\right) = -\frac{E_k}{kT} \quad (1)$$

where I_{kl} is the emission intensity of a transition between the upper energy level k to the lower level l at wavelength λ , g_k is the statistical weight factor and E_k the energy of the excited state, A_{kl} is the Einstein transition probability and k is Planck's constant.¹ Plotting line intensities of an element against the energy of the excited state provides the temperature.

For reliable determination of the temperature the plasma should be in local thermodynamic equilibrium (LTE), which means that the electron collision rate processes should dominate radiative decay and recombination.⁴⁰ In addition to the lack of LTE in the measurements, uncertainties in temperature determinations arise also from the inaccuracies of the reported values for transition probabilities, which can vary up to 50 % depending on the transition.⁴¹ Also the limited information of the transitions, especially in the VUV, complicates the plasma temperature determinations. Therefore the temperature of plasmas generated by ArF and KrF excimer lasers were analyzed in the visible spectral range for copper and copper carbonate hydroxide. The six copper emission lines used to determine the temperatures in both samples are presented in Fig. 9 and the data of the transitions is given in Table 1.

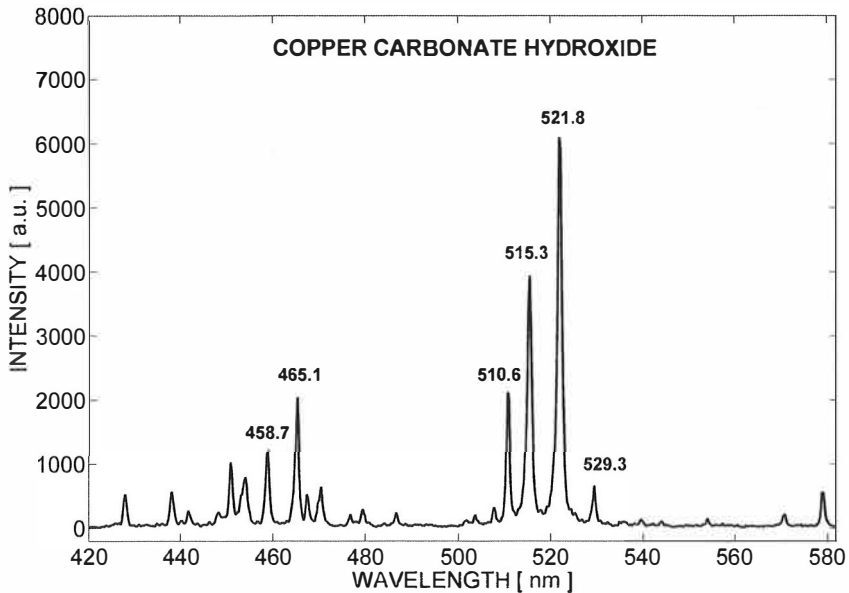


FIGURE 9: Copper emission lines for the estimation of plasma temperature in metallic copper and copper carbonate hydroxide samples. Spectrum was measured from copper carbonate hydroxide sample with a delay time of 150 ns and measurement gate width of 100 ns. Plasma was created with 10 KrF laser pulses of 0.45 mJ pulse energy and a spot size of $\sim 1.0 \times 10^{-4} \text{ cm}^2$.

TABLE 1: Parameters of the spectral transitions of copper used in the temperature determinations.⁴¹ Emission lines at 521.82 nm and 522.01 nm could not be resolved in the spectra and therefore only data of 521.82 nm having higher transition probability A_{ki} was used in the fitting. For all these transition probabilities $\Delta A/A$ was 25%.

λ [nm]	E_k [cm^{-1}]	g_k	A_{ki} [10^8 s^{-1}]
458.70	62 948	6	0.320
465.11	62 403	8	0.320
510.55	30 784	4	0.020
515.32	49 935	4	0.60
521.82	49 942	6	0.75
522.01	49 935	4	0.150
529.25	62 403	8	0.109

A typical Boltzmann plot for copper carbonate hydroxide using the background corrected emission lines from Fig. 9 is presented in Fig. 10, giving the plasma temperature of $\sim 11\,200$ K. The plasma temperature for metallic copper measured under same conditions was $\sim 13\,150$ K. Plasma temperatures as a function of laser irradiance for both lasers in metallic copper and copper carbonate hydroxide are shown in Fig. 11. The temperature increased almost linearly, when the irradiance was varied in this range. However, the errors in the temperatures for both samples, estimated from the fitting, increased from of the order of 3 % to 13% at the lowest and highest irradiance, respectively. It indicates that requirements of LTE and optically thin plasma are not fully realized at high irradiances at the short measurement delays used in the study. For both excimer lasers the similar behavior was observed; the temperature for the metallic copper was higher than that for the copper compound. In a study of copper in ArF laser generated plasma with 100 mJ pulse energies Lee *et al.*⁴² obtained temperatures varying from 13 200 K to 17 200 K, depending on the measurement point in the plasma plume. Higher temperature values obtained for copper in that study were most likely caused by higher laser irradiance ($\sim 2 \text{ GW cm}^{-2}$) at the sample.

For metallic copper the temperature of ArF laser-induced plasma is lower than that of the KrF laser generated plasma. The lower plasma temperature in case of ArF may be caused by more efficient scattering of the fewer, but more energetic, photons by the plasma. Also the plasma heating via IB can be stronger at 248 nm than at 193 nm. Nevertheless, these effects should influence also the temperatures determined from copper carbonate hydroxide and therefore the difference in the temperature can not be explained further by the current data only.

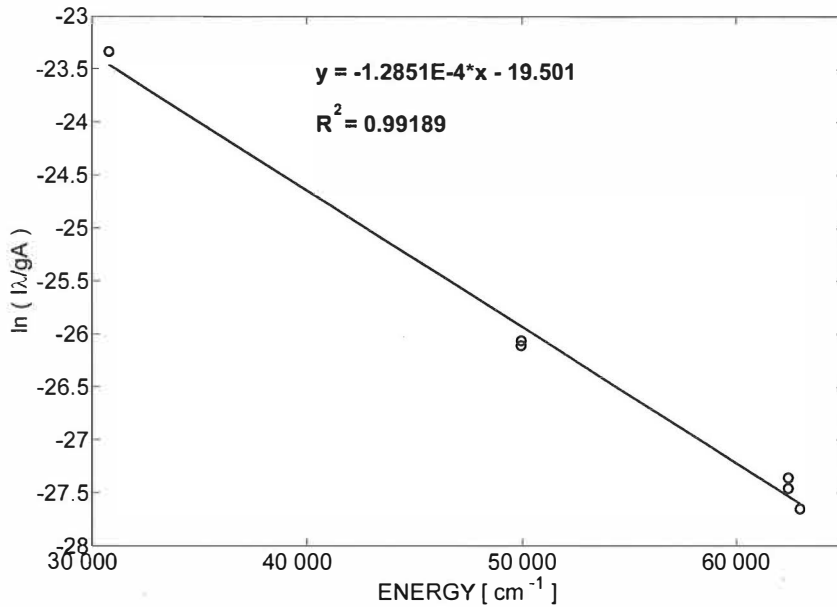


FIGURE 10: A Boltzmann plot for the copper carbonate hydroxide plasma temperature determination using six copper emission lines presented in Fig. 9.

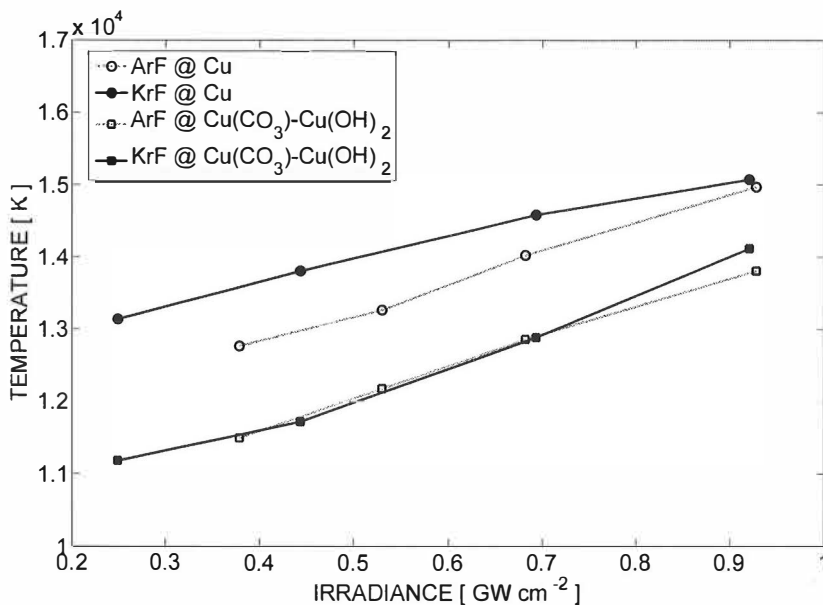


FIGURE 11: Plasma temperature as a function of laser irradiance in metallic copper and copper carbonate hydroxide. Spot size at the sample was $\sim 1.0 \times 10^{-4} \text{ cm}^2$ for both lasers. Delay and gate times were 150 and 100 ns.

2.2.4 Plasma shielding

In a process called plasma shielding, the energy of the incident laser pulse is attenuated by the plasma plume due to absorption and scattering. The plasma shielding is more effective at same irradiances with larger spot sizes due to increased volume of the ablated species along the beam path.⁴³ Also the pulse duration affects to shielding because of the longer interaction time and as a special case, plasma shielding is considered negligible with ultrashort laser pulses, because the laser energy is deposited to the sample before plasma expansion. The plasma shielding has been generally considered less severe at UV wavelengths, because the laser energy is absorbed to the plasma by IB processes, where the electron cascade growth rates are proportional to λ^3 .²³ However, the probability for scattering by the ablated particles is higher at short wavelengths. In graphite targets the increase of irradiance of Nd:YAG laser at 1064 nm has been observed to decrease the particle size.⁴⁴ Thus at high irradiances with UV wavelengths the scattering can be even stronger than at lower irradiances. Also the absorption of UV wavelengths is stronger during the plasma evolution, because the absorption probability in IB is highly dependent on the electron concentration in the plasma and in fact photoionization processes provide high electron concentrations.²⁵

Plasma shielding was studied in paper IV with ArF and KrF laser-induced plasmas in a pure copper sample. The strongest emission lines of copper are located around 325 nm; however, they suffer significantly from self-absorption at high irradiances. Therefore, copper emission was detected in the range between 430 nm to 560 nm because of the non-resonance transitions there.

There was no difference between emission lines regarding the attenuation of the emission intensity due to the plasma shielding, and therefore only the strongest peak at ~522 nm was used in the analysis. Irradiance at the sample was varied by changing the lens-to-sample distance with a 40-mm focal length lens. Optical attenuator was used to control the laser pulse energy at the sample. The intensity profiles of the copper line against the irradiances as a function of LTSD are presented in Fig. 12. At the focal point (Δ LTSD=0) the irradiance was highest, but the maximum emission intensity for both lasers was not observed this location, when high irradiances were used because of plasma shielding. A similar behavior of the intensity maximum location has been also observed in a study with a Nd:YAG laser.⁴⁵ Below the threshold value of ~1 GW cm⁻² the influence of plasma shielding was not observed in LIPS intensities in either laser in the present work.

According to the intensity profiles, the threshold irradiance for both lasers in generation of the plasma at copper was of the order of 0.1 GW cm⁻². The value is comparable to the plasma threshold irradiance, ~0.3 GW cm⁻² measured with Nd:YAG laser at 532 nm in other LIPS studies.^{46,47} However, the plasma threshold can somewhat vary with the laser wavelength, because the absorbance of the sample depends on the wavelength.

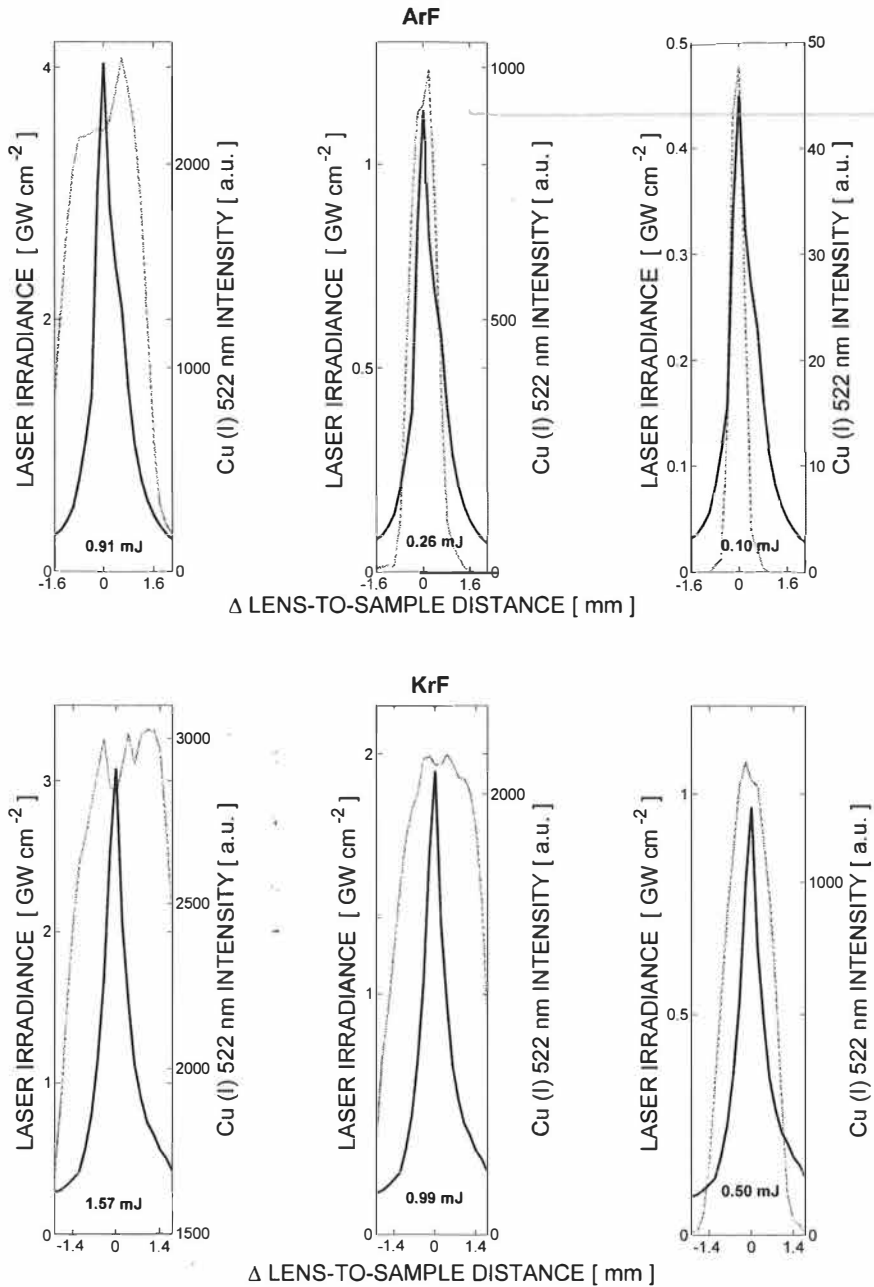


FIGURE 12: Intensity profiles of copper (gray) and the calculated laser irradiance at the sample (black) as a function of the lens-to-sample distance for (1) ArF and (2) KrF laser. Negative and positive LTSD values indicate focusing inside and in front of the sample, respectively. The delay and the gate times were 100 ns.

The attenuation of the emission intensity due to plasma shielding was observed also at longer delays (see Fig. 13). The width of the intensity profile is decreased at the longer delay times. This is due to the faster decay of the emission intensity at larger LTSD values having a smaller irradiance, as indicated by previous study, where temporal behavior of intensities as a function of laser irradiance was studied.⁴⁸ At longer delay times emission intensity was observed in Fig. 13 only from smaller spots near the focal area and therefore rather short delays were used throughout the study presented in paper IV.

Although the lifetime of the plasma at low pulse energies used in this study is a lot shorter than the time delay between the consecutive laser pulses (at 15 Hz ~70 ms), at high repetition rate there can still be some particles originating from the previous ablation process, which may cause scattering and absorption. Small particles may initiate plasma already in the gas above the sample surface, and thus diminish the amount of energy coupled to the sample. However, the influence of the repetition rate to the LIPS signal was not significant in this study and it was observed only at the focal area.

Influence of the argon atmosphere to the plasma shielding was also investigated (see Fig. 14). Stronger shielding, especially in the direction of positive LTSD values, was observed, when argon flow towards the plasma was applied. This can be caused by the breakdown of argon, which has been observed before the main plasma at different focusing distances of a Nd:YAG laser by Aguilera *et al.*⁴⁹ Also the inverse bremsstrahlung has been observed to be most effective in argon.³⁰ Therefore the argon atmosphere can simultaneously both increase and decrease the emission intensity observed in LIPS due to higher plasma temperature and stronger plasma shielding, respectively.

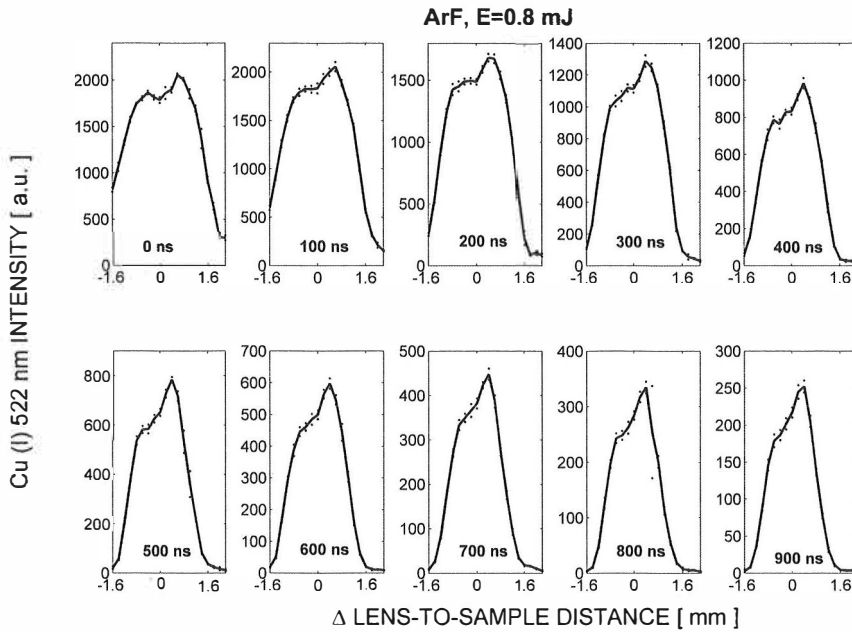


FIGURE 13: Influence of the measurement delay to the copper emission line intensity profile at the ArF laser energy of 0.8 mJ. The measurement gate width was 100 ns. The errors were estimated as a standard deviation of 5 measurements.

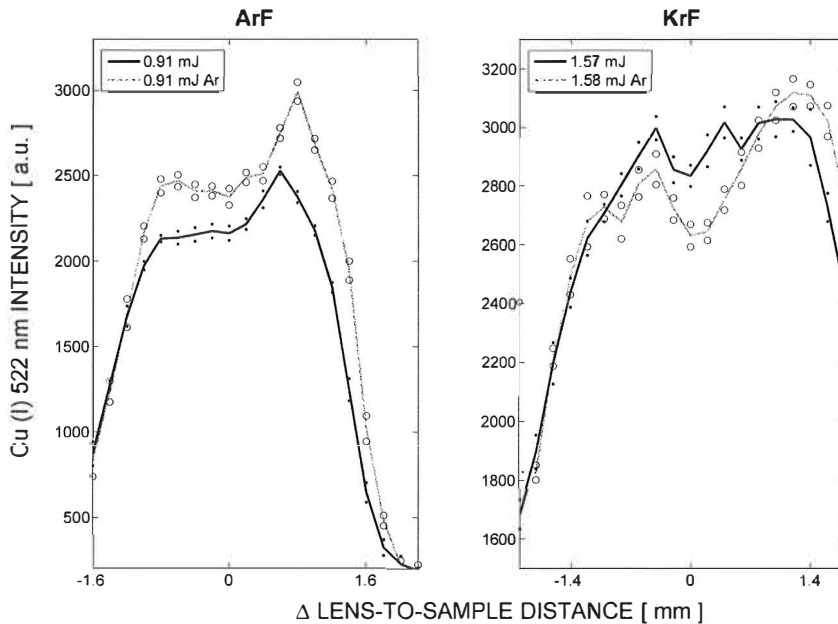


FIGURE 14: Influence of argon to the copper emission line intensity profile (gray) in comparison to profile measured in air (black). Maximum irradiance was ~ 4 and ~ 3 GW cm⁻² for ArF and KrF, respectively. The measurement delay and the gate width were 100 ns. The errors were estimated as a standard deviation of 5 measurements.

3 MEASUREMENTS IN VACUUM ULTRAVIOLET

3.1 Preventing atmospheric absorption in LIPS analysis

Spectral region from 100 nm to 200 nm is known as vacuum ultraviolet, VUV, because the radiation at wavelengths <200 nm is strongly absorbed by air. The Schumann-Runge bands of molecular oxygen below 200 nm are mainly responsible for the atmospheric absorption. Nitrogen is practically transparent for VUV radiation down to 100 nm, but carbon dioxide absorbs emission below 165 nm. Also water vapor absorbs radiation between 155 nm and 180 nm, and below 140 nm.⁵⁰ The spectroscopic measurements in the VUV have to be carried out in vacuum or in suitable gas atmosphere, for instance in nitrogen, argon or helium. In addition to prevent the atmospheric absorption in LIPS gas chambers are used also to enhance the signal by inert gas in other spectral regions, as already discussed in previous chapters.

Vacuum techniques have been used in LIPS measurements of solid steel in VUV, from which *e.g.* carbon and sulfur have been detected in the region from 40 to 160 nm with a photodiode array detector.⁵¹ Instead of high vacuum, the sample has also been installed to a chamber containing buffer gas and VUV transparent windows, again for analysis of solid steel.⁵²⁻⁵⁷ A special immersion lance for LIPS analysis of liquid steel has been developed for measurements, in which the lance is cooled with water flow and the optical path between the plasma and collecting lens has been flushed with argon gas. The gas flow also protected the lens against dust and splashes of the melt.¹¹

Different purging arrangements of the optical paths have been applied in LIPS analysis of sulfur in rubber,³⁰ solid steel,⁵⁸ and sulfuric acid aerosols.⁵⁹ In all the above-mentioned experiments the spectrograph has either been in vacuum or filled with inert gas, most often nitrogen. Recently VUV spectral range has also been applied to analysis of brominated thermoplasts⁶⁰ and geological samples to demonstrate the potential of the method for space exploration.⁶¹ In both studies a gas chamber was used, in the former case filled with in argon and in the latter with CO₂ at reduced pressure to simulate the Martian atmosphere.

In this work the atmospheric absorption has been eliminated with a gas flow through the spectrograph, but also a sample chamber has been used. The purging arrangements used in the study are illustrated in Fig. 15. The Czerny-Turner spectrograph was purged with nitrogen or argon through the inlet installed to the lid of the spectrograph. Inert gas replaced air inside the spectrograph after a few minutes of moderate flushing. A gas flow through the spectrograph purged the optical path between the plasma and the entrance slit. The sample was positioned close to the slit with an average distance of 10 – 20 mm. Metal cover with a small hole in front of the slit lead the gas flow effectively towards the sample. The influence of the atmospheric absorption on emission line intensities below 190 nm is illustrated in Fig. 16. The emission lines of nickel can barely be detected around 185 nm in air, while under nitrogen and argon purge intensive emission is detected. The significant enhancement of the emission intensities, as well as the increased background in argon, can be observed in the spectra measured under same experimental conditions.

A small sample chamber (50 mm × 50 mm × 50 mm) manufactured from stainless steel has also been used. The quartz window of the chamber was used for the laser input and the magnesium fluoride window for detection of emission. The chamber was first evacuated and filled with argon to a reduced pressure and placed close to the entrance slit of the spectrograph. The changing of the sample was, however, slow in this setup. The emission signal level was somewhat lower, because the distance between the plasma and the slit was longer than in the direct purging arrangement.

It was also demonstrated, that optical fiber bundle made from UV-grade fused silica could be used in the VUV measurements down to 180 nm. In measurements using optical fiber cost effective nitrogen could be used in the spectrograph and argon flow at the front end of the fiber. Argon flow towards the sample through a metal cover at the end of the fiber purged the optical path between the fiber end and the plasma. Such arrangement can be also used to enhance signal intensity in other measurements in UV and visible regions. The fiber end was installed close to the sample and therefore no vigorous gas flow was needed. However, the signal is considerably attenuated by the fiber already before the cutoff limit and therefore direct measurement of the plasma plume is recommended for measurements of low concentrations samples or weak emission lines.

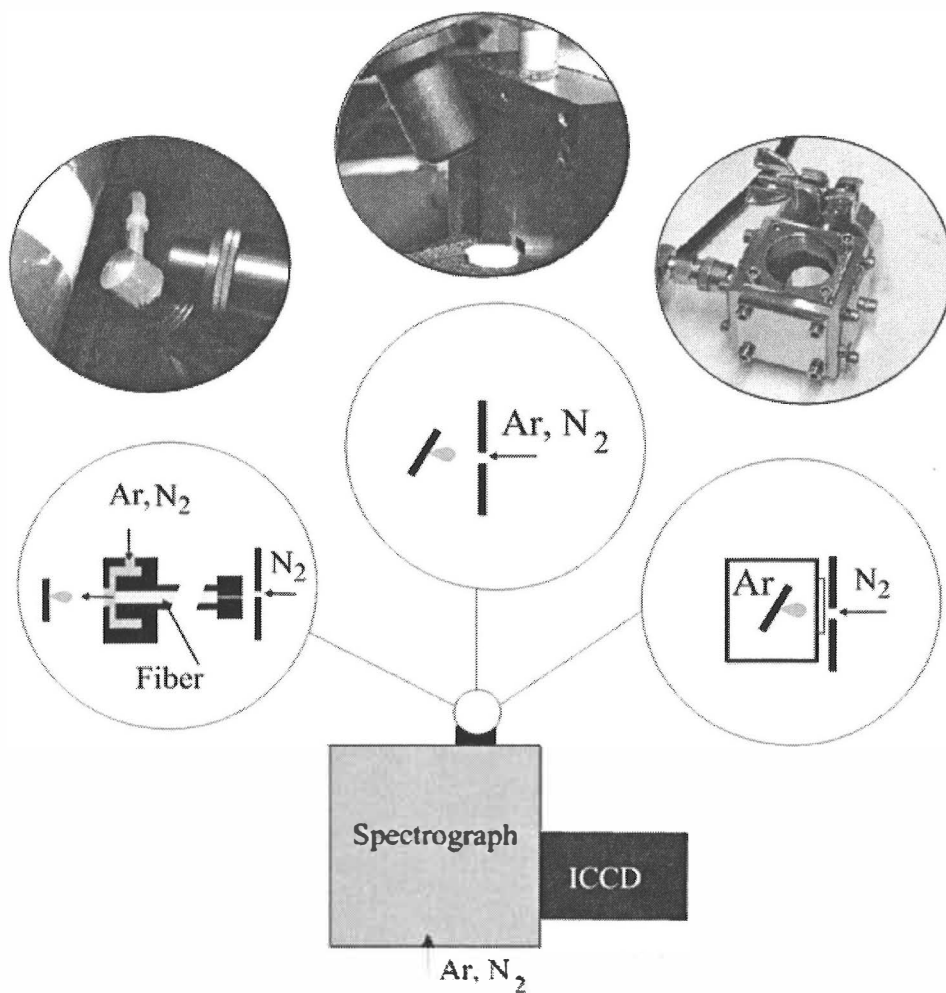


FIGURE 15: Purge systems to prevent atmospheric absorption. In the photograph at left the metal cover with a gas inlet for optical fiber is shown. In the middle picture the purge gas flows from the slit of the spectrograph towards the plasma and the sample is in front of the slit. On the right picture the sample is installed into a chamber, which can be used at reduced pressure, with VUV transparent windows. The diagrams describe the various purge geometries at the slit of the spectrograph.

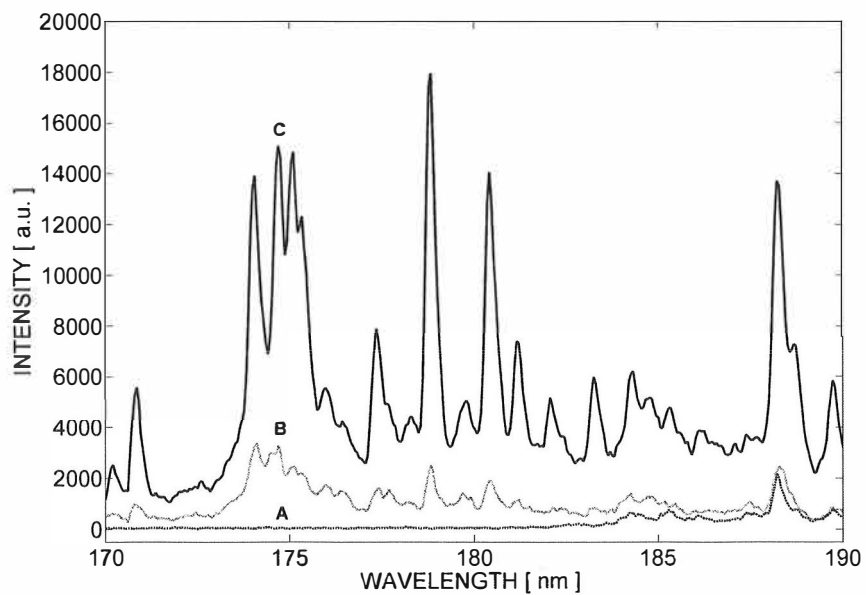


FIGURE 16: Emission spectrum of pure nickel measured from ArF excimer laser generated plasma (A) in air (B) under N_2 flow and (C) under argon flow with 10 laser pulses. Delay time was 100 ns and the measurement gate width was 500 ns.

3.2 Detection of the plasma emission in vacuum ultraviolet

The applicable optics and instrumentation in VUV has to be considered carefully, as the regular optics can not be used in the VUV region. A thin layer of high quality fused silica transmits down to 165 nm, but the selection of other available materials for VUV optics is limited, see Table 2. Regardless of the low nominal cutoff limit, the material can absorb significantly already at longer wavelengths. For example, the UV grade fused silica lens used in this study, absorbed ~20 % of the ArF laser pulse energy. For KrF laser the corresponding value was ~10%. Transmission at shortest wavelengths is obtained with fluorides, but as material they are technically more demanding due to the crystalline form and they can also be susceptible to thermal shock. There is no practical material that would widely transmit at range below ~105 nm, *i.e.*, cutoff for LiF. Nevertheless, very thin foils of some metals like aluminum or indium can be applied at certain wavelength ranges in EUV. In mirrors and reflective gratings, aluminum coated with VUV transparent material (e.g. MgF₂) can provide ~70% reflectivities down to 115 nm.⁶²

TABLE 2: Transmission cutoffs of materials used in VUV optics and windows. ⁶²

Material	Cutoff
LiF	105 nm
MgF ₂	115 nm
CaF ₂	123 nm
SrF ₂	128 nm
BaF ₂	135 nm
Al ₂ O ₃ (sapphire)	145 nm
SiO ₂ (UV-grade)	165 nm

3.2.1 Spectrographs

With a specially designed VUV spectrograph lines down to 40 nm have been measured in LIPS applications under vacuum conditions.⁵⁶ Recently the use of an echelle type spectrograph in VUV range down to 150 nm has been demonstrated.⁶³ In the present work the plasma emission was dispersed in a 150 mm Czerny-Turner type imaging spectrograph (Acton, SP-150). The holographic UV-grating used in the VUV measurements contained 2400 grooves per millimeter. The working range for the grating used was 190-450 nm according to the manufacturer. Neither the mirrors of the spectrograph nor the grating were designed for VUV spectral range. Nevertheless, the performance of a common spectrograph in VUV detection was demonstrated. The small volume of the spectrograph container enabled fast replacement of air with a purge gas. The lowest emission lines detected with the spectrograph were located at ~130 nm (see paper I) although the transmission efficiency of the grating was low in the region. Only the plasma temperature and the plasma shielding measurements were carried out in the visible and then a grating having 600 grooves per millimeter and blazed to 200 nm was used.

3.2.2 Detectors

Usually in the LIPS measurements the emission is detected with a photomultiplier tube (PMT), a photodiode array (PDA), or a charge-coupled device (CCD). While PMT is highly sensitive in detection of UV and visible radiation with extremely fast response time, several PMTs have to be used for simultaneous multi-element analysis. In LIPS measurements the potential to detect multiple emission lines simultaneously is a significant advantage, which can be obtained solely with PDA or CCD detectors. These multichannel detectors offer also linear response in a wide spectral range with low noise and dark current and they have large dynamic range. Especially the sensitivity and the possibility for time-gated detection with intensified charge-coupled devices (ICCD) enable measurements at optimal phases of plasma evolution. In an ICCD the sensitivity of the detector is enhanced with a micro-channel plate (MCP), which multiplies the number of electrons arriving from the photocathode. The cloud of electrons is converted at a phosphor coating into light, which can be recorded with a CCD. In addition to the increment in the intensity, the image intensifier allows also very fast gating at time-scales of 5 to 10 ns. In a LIPS study where ICCD was compared to non-intensified, gated CCD detector, the former detector has been observed to offer significantly better temporal and spectral resolution, sensitivity and dynamic range.⁶⁴ The spectral response of an ICCD is determined on the by the input window material of the intensifier and the photocathode, from which the input window determines usually the lowest detectable wavelength.⁶⁵

In paper I the performance of two different ICCDs in VUV LIPS measurements was demonstrated. Only recently the use of ICCD detector in VUV spectral region has been reported in other LIPS studies.^{61,63} In the current work one ICCD was equipped with quartz input window and another with a MgF₂ input window. Quartz window enabled detection in the spectral ranges of 164-850 nm and MgF₂ window in the range of 130-850 nm. Both detectors had 1024 × 256 pixel imaging area and a 18-mm image intensifier. The attenuation caused by the quartz input window in ICCD detection is shown in Fig. 17.

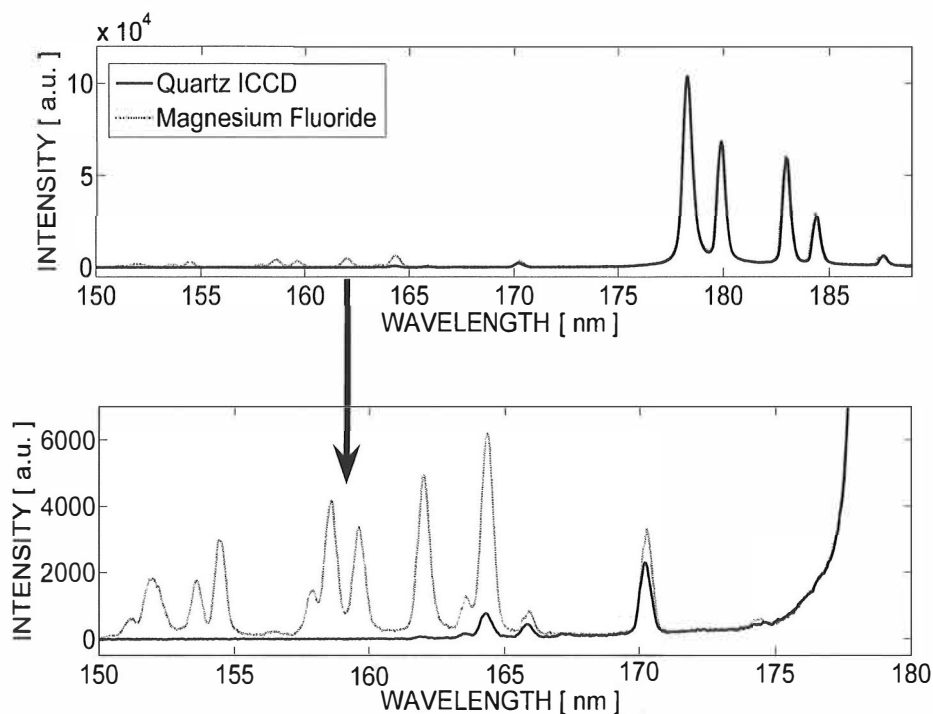


FIGURE 17: Attenuation of the emission in ICCD containing quartz input window. Spectra were measured from a mixture of potassium iodine and potassium bromide salts in argon with 10 pulses from ArF excimer laser. The delay time was 100 ns and the gate width was 1000 ns.

4 LIPS STUDIES IN VACUUM ULTRAVIOLET

4.1 Sulfide minerals

4.1.1 LIPS in analysis of geological samples

In analysis of geological samples the minimal sample preparation for LIPS measurements is a benefit, when a large number of samples are to be analyzed. On the other hand, the material to be analyzed is inhomogeneous: rock samples consist of countless number of small mineral crystallites, and finding a suitable set of calibration samples can be time-consuming, if not impossible. Hence the question of representative sampling has to be studied carefully in quantitative analysis of geological samples. Grinding of the samples has been considered as a one solution in getting a representative mineral composition in the LIPS analysis.⁶⁶⁻⁷⁰ Also collecting a large number of sampling points have been considered. For example, spectra for quantitative analysis have been collected as an average over sampling points within lengths of 0.2 m - 2 m from a drill core sample.⁷¹ On the other hand, information of the distribution of the elements in sample can reveal the origin or the geological history of the sample and therefore also mapping of geological samples have been found useful.⁷²⁻⁷⁶

The future use of LIPS to the analysis of rock and soil samples at the planets has also been studied by several groups.^{34,77-79} Recently also the usability of VUV spectral range under Martian conditions has been demonstrated in analysis of geological samples.⁶¹

4.1.2 Analysis of drill core samples in VUV

Drill core samples are used routinely in mining industry for the exploration of new ore locations or for the sampling from an existing ore deposit. Tens of meters of drill core can be collected daily from different locations and depths. Main ores in the sample are identified visually by a geologist and for the further analysis the core is split and one half is sent to analytical laboratory. Because thorough laboratory assays are time-consuming and expensive, all drill core samples can not be sent to laboratory analysis. It has been suggested, that LIPS could be applied to quantitative on-line analysis of minerals in drill core samples.⁷¹ Good linear correlation of emission intensities against laboratory assays were obtained in that study for Cr, Cu, Fe, Mn, and Ni ($R^2=0.92-0.99$), which were present at levels of 0.02% to 10%. However, the results showed only semi-quantitative analytical potential, because of the different sampling statistics in LIPS and laboratory assays and the highly inhomogeneous composition of the samples.

If exact quantitative results are not of concern, rapid LIPS measurements combined with an automatic identification of economically interesting ores could be used in on-line sorting of the drill core samples for the further laboratory analysis. In paper II the potential of LIPS method for identification of minerals using VUV detection was demonstrated. Vacuum ultraviolet offers a suitable spectral range for identification of commercially important sulfide minerals. In Finland copper, zinc and nickel are most important metals refined from sulfide minerals. The strongest emission lines of sulfur are located ~180 nm, while the visible spectral range contains only some weak emission lines at ~415 nm and ~458 nm. Strong sulfur lines can be found in the near infrared region at ~920 nm, but it is out of the detection range of most ICCD detectors. It can be noted, that the VUV lines can be detected also with a purged UV-grade optical fiber presented in paper I, but only in high concentrations. In principle, the direct purge trough the spectrograph is a convenient option, allowing also measurements of samples containing only small amounts of sulfur.

Pieces of halved drill core samples (<15 cm in length) containing sulfide minerals were obtained from the Pyhäsalmi mine, which has been in production since 1962 and is the biggest mine in Finland. The rough composition of the samples according to geological analysis is presented in Table 3.

TABLE 3: Drill core samples from Pyhäsalmi mine used for LIPS analysis.

Sample	Main mineral(s)	Other
2505/1.3	(Zn,Fe)S, FeS ₂	BaSO ₄ , CaCO ₃ , Mg,Ca(CO ₃) ₂
2505/5.4	(Zn,Fe)S	plenty of BaSO ₄ , CaCO ₃ , Mg,Ca(CO ₃) ₂
2505/39	FeS ₂ , CuFeS ₂	CaCO ₃ , Mg,Ca(CO ₃) ₂
2505/58	FeS ₂	CuFeS ₂ , CaCO ₃ , Mg,Ca(CO ₃) ₂
2505/68.5	FeS ₂ , CuFeS ₂ , (Zn,Fe)S	Heterogeneous sample

LIPS analysis from the surface of the drill core sample was carried out at 250 sampling points along a 5 cm line. The mineral in each sampling point was determined by using reference spectra of the main minerals in the sample (see Fig. 18). The reference spectra were measured from ore grains at known mineral composition but barite (BaSO₄) and calcite (CaCO₃) were measured from pure compounds. The optimal spectral region for the analysis of the drill core samples was found between 170 and 210 nm. All the main minerals had a characteristic emission spectrum in this region except pyrite (FeS₂) and pyrrhotite (FeS). These minerals differ only by the relative emission intensities of sulfur and iron.

The spectra were measured under nitrogen purge, because it would be cost-effective in industrial use for mineral sorting. Atomic nitrogen has strong emission peak around 174.2 nm, but it was not dominating in any spectra recorded (see Fig. 18). All spectra were normalized to their total intensity for the identification procedure, since the intensity levels of the spectra varied from point to point due to different materials and possible laser energy fluctuations.

Linear least square fitting of the each measured spectra against the reference spectra set was carried out by using the *lsqnonneg* -function in Matlab software package (Mathworks, Inc). The reference mineral having a highest fitting coefficient was chosen as a representative of that sampling point, if its coefficient would differ more than 5% from the following coefficient. A constraint of nonnegative coefficients was set to the fitting procedure to simplify the interpretation of the results. It was observed, that it was not possible to automatically distinguish pyrite from a pyrrhotite in this fitting. Identification of chalcopyrite from these two was also difficult based from the fitting coefficients, as the three spectra are similar. Other four reference minerals were easily distinguished by their fitting coefficients, if the sampling point contained the mineral. Therefore if the highest fitting coefficients were obtained for FeS, FeS₂ and CuFeS₂, an additional fit to a spectrum against the reference spectra of only these minerals was carried out in order to identify the mineral correctly.

The quality of the drill core samples can be judged from the mineral distribution graphs (Fig. 19). For example, the sample 1.3 is optimal if the main interest is the sphalerite. On the other hand, the sample 5.4 contains only a very small amount of chalcopyrite. Samples 39 and 58 are rich in pyrite, while in sample 68.5 a considerable amount of dolomite was identified.

For some spectra the identification procedure did not work. When the measured spectra did not clearly match any of the seven reference spectra, all coefficients were close to each other. It has to be reminded, that the fitting was carried out against the main minerals in the sample, only. Also when the sampling point was at the boundary region of two or more mineral grains, the spectrum was clearly a superposition of two or more reference spectra and therefore the coefficients were too close to each other to be confidently classified to one mineral, only. The percentage of non-classified sampling points varied from 4 to 12 depending on the sample (see bar A in Fig. 19).

More representative analysis would need a denser sampling than in this study and larger reference spectra library. However, the emphasis of this work was to demonstrate the potential of LIPS for mineral identification, and thus more efficient algorithms and programs for the spectra processing could be selected for the real application. Moreover, the experimental instrumentation should be specially designed for the harsh mining conditions. By choosing a high power industrial laser the spot size at the sample could be increased without reduction of the signal intensity. The experimental setup presented in paper II would offer at best a sampling rate of 1 cm/s and even higher rates could be obtained with different detection schemes. In these demonstrative measurements the performance of the detector limited the repetition rate of the laser to 15 Hz in order to minimize the background noise from the readout of the data.

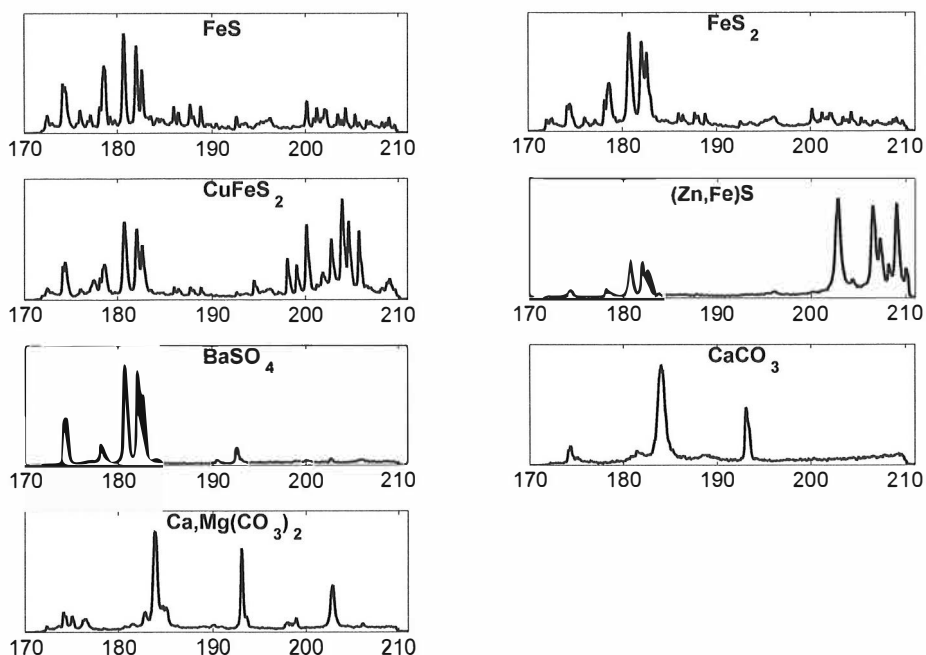


FIGURE 18: Reference of the main minerals found from the drill core samples.

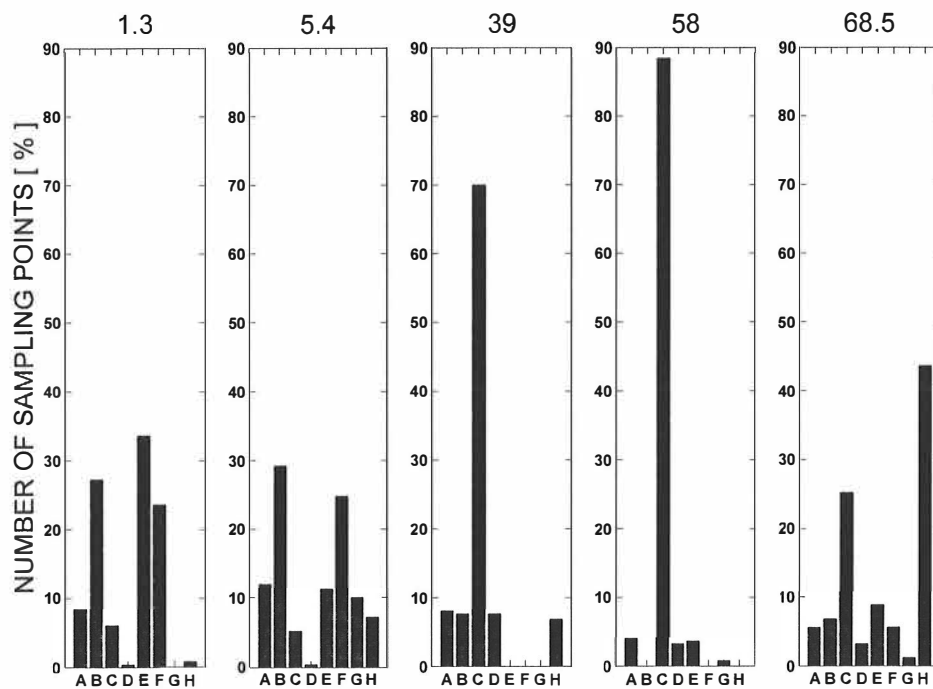


FIGURE 19: Mineral distribution in drill core samples according to the LIPS measurements from 250 sampling points. Letter A stands for the percentage of the points, which could not be classified, B is pyrrhotite FeS, C is pyrite FeS₂, D is chalcopyrite CuFeS₂, E is sphalerite (Zn,Fe)S, F is barite BaSO₄, G is calcite CaCO₃ and H is dolomite Ca,Mg(CO₃)₂. The numbers above the panels refer to the different samples.

4.2 Chlorinated and brominated organic compounds

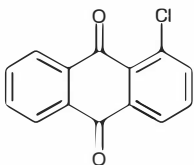
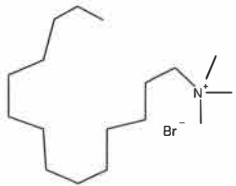
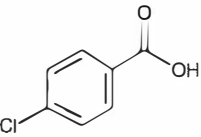
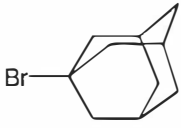
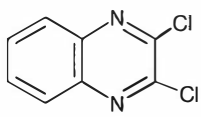
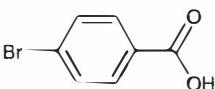
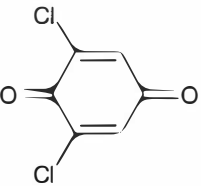
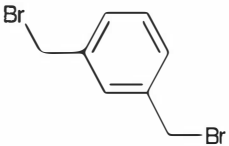
4.2.1 LIPS in analysis of chlorine and bromine

The most sensitive emission lines of chlorine and bromine fall in the VUV spectral region. Some lines of these halogens are also found in the NIR region; strongest around 837 nm and 830 nm for chlorine and bromine, respectively. Previously the LIPS analysis of chlorine has been carried out in the NIR spectral region and it has been detected from air,⁸⁰⁻⁸³ exhaust fumes,⁹ liquids,^{84,85} polymers,⁸⁶ solid organic compounds,^{87,88} pharmaceutical products,⁸⁹ and geological samples.^{61,78} The NIR region has been used as well in the on-line detection of bromine from polymers.¹² Only recently the VUV spectral range has been applied to analysis of chlorine⁶¹ or bromine⁶⁰ in addition to this work. Several emission lines occur in the UV and visible spectral range for both halogens,⁴¹ they have shown too small intensities to be utilized in LIPS analysis.^{60,81}

4.2.2 Analysis of solid organic compounds

Chlorinated and brominated organic compounds are used in industry for example in production of polymers, synthetic solvents, pesticides, pharmaceuticals, dyes, disinfectants *etc.* Because some chlorinated and brominated organic compounds tend to be persistent and accumulative in biological tissues their analysis is of great interest in environmental sciences, especially in soil samples. Analysis of halogenated solid organic compounds with LIPS method was first reported by Tran *et al.* in the NIR spectral region.⁸⁷ In paper III analysis of chlorine and bromine in solid organic compounds was carried out in VUV spectral region, and the practical limits of the gas-purged setup in detection of halogens were observed. The solid compounds selected for the analysis are presented in Table 4. The emission line of chlorine at 134.7 nm and bromine at 154 nm were chosen for the analysis (see Fig. 20 Carbon emission peaks at ~143 nm and at ~156 nm were used as an internal standard in the analysis of chlorine and bromine, respectively. Emission lines of the major constituent of the sample has been used to internal standardization in carbon-rich materials,^{87,89,90} but also in other samples.^{11,66,91-93} The procedure improved the linear correlation of the emission intensities against the atomic ratio ratios, especially in samples containing chlorine in the present work.

TABLE 4 : Structures of the solid organic compounds analyzed in paper III.

Compound	Structure	Compound	Structure
1-Chloro-9,10-anthraquinone $C_{14}H_7ClO_2$ $M_w=242.66$ g/mol		Tetradecyl-trimethyl-ammonium-bromide $C_{17}H_{38}NBr$ $M_w=336.41$ g/mol	
4-Chlorobenzoic acid $C_7H_5ClO_2$ $M_w=156.57$ g/mol		1-Bromo-adamantane $C_{10}H_{15}Br$ $M_w=215.13$ g/mol	
2,3-Dichloro-quinoxaline $C_8H_4Cl_2N_2$ $M_w=199.04$ g/mol		4-Bromobenzoic acid $C_7H_5BrO_2$ $M_w=201.02$ g/mol	
2,6-Dichloro-1,4-benzoquinone $C_6H_2Cl_2O_2$ $M_w=176.98$ g/mol		1,3-Bis(bromomethyl)-benzene $C_8H_8Br_2$ $M_w=263.96$ g/mol	

The normalized halogen/carbon intensity ratios did not give linear correlation against the atomic ratio ratios under nitrogen purge (Fig. 21). Part of the scattering of the data is most likely related to the turbulent nitrogen flow between the plasma and the slit of the spectrograph, because the atmospheric absorption is already severe at this spectral region. On the other hand, the nitrogen can dissociate and form reactive radicals in the plasma and can consequently generate molecules especially with atomic carbon abundant in the plasma. As an indication of such reactions, where molecules are formed, is the relative halogen/carbon intensity ratio that is higher in nitrogen flow than in argon chamber. However, the reproducibility of the measurement under argon flow was not significantly better because of the interference of atmospheric absorption. Therefore a chamber filled with argon was used in the measurements. Reduced pressure of ~70 mbar was observed to give optimal emission intensities.

The least square fitting of the results in argon atmosphere (see Fig. 4 in paper III) gave a limit of detection (LOD) for chlorine and bromine 0.054 and 0.011, respectively, expressed in halogen/carbon ratio. In the NIR region study by others,⁸⁷ the corresponding detection limits measured in air were 0.011 and 0.0028 for chlorine and bromine, respectively, and in helium flow the LOD values were approximately magnitude smaller. Higher LOD values obtained in the present study can be described to be caused by the low transmission efficiency of the conventional spectrograph at these VUV wavelengths. However, according to the present results compounds containing 90 carbon atoms against one bromine atom can be determined from their bromine/carbon ratios. For chlorine compounds the respective ratio was 20:1. For practical analysis of chlorine at least a grating optimized for VUV analysis should be used. Nevertheless, both elements can be measured also with the experimental setup used, when the concentration of the element is high enough in the sample.

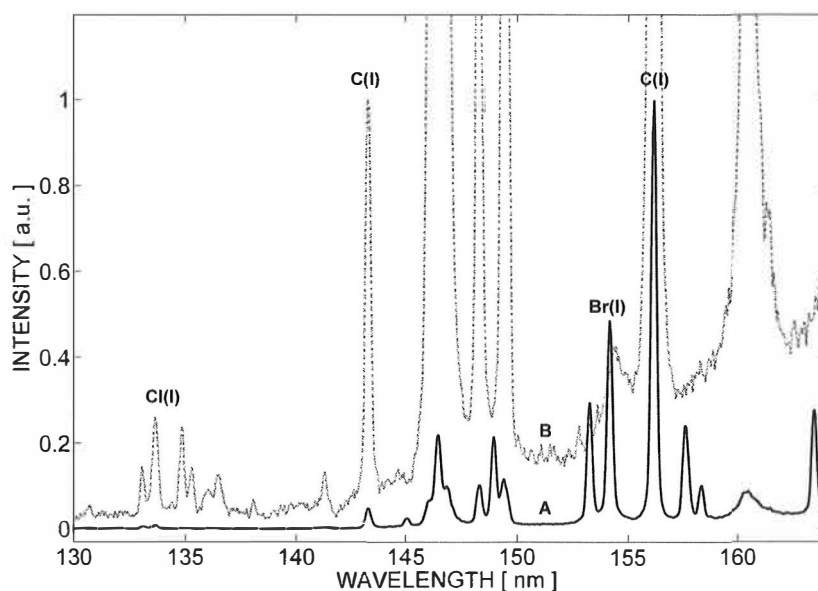


FIGURE 20: Normalized spectrum of (A) 4-bromobenzoic acid (black) and (B) 1-chloro-9,10-anthraquinone (gray) showing the emission lines used in the analysis of halogenated organic samples.

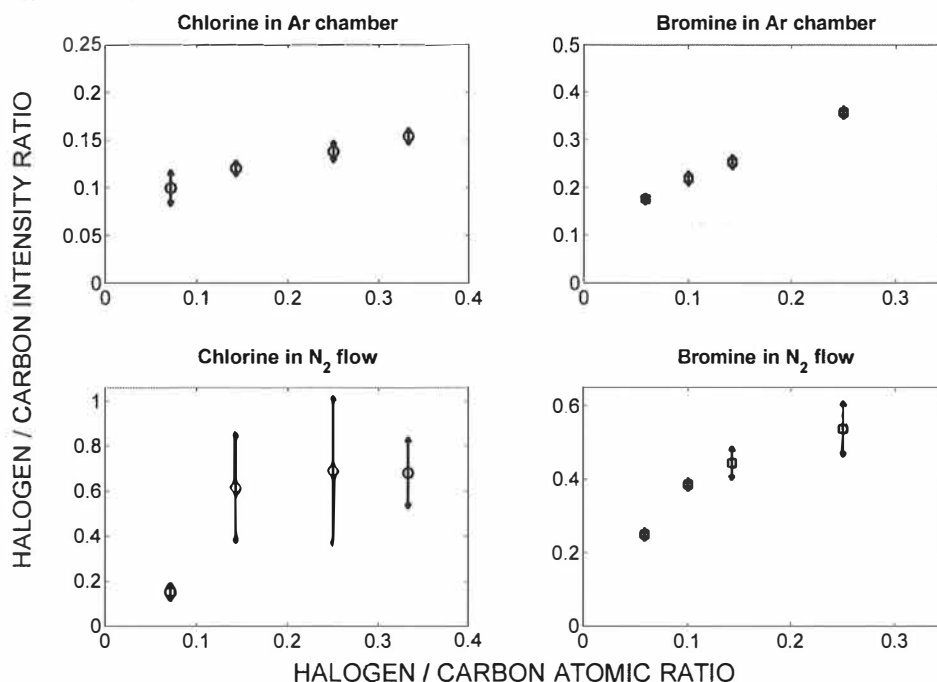


FIGURE 21: Influence of purging to the halogen/carbon intensity ratios. Plasma was generated with KrF excimer laser at an irradiance of $\sim 2 \text{ GW cm}^{-2}$. Error bars are standard deviations of the intensities between 5 sampling points. The optimal delay time in nitrogen flow was found to be 50 ns, while in Ar chamber at ~ 70 mbar pressure the respective delay time was 150 ns. Measurement gate width was in 500 ns in both cases.

5 SUMMARY

A new approach to laser-induced plasma spectroscopy, LIPS, in the vacuum ultraviolet spectral region, *i.e.*, below 200 nm, has been introduced in this thesis. Several non-metallic elements (S, Br, I, P, C, As, Cl) have intensive emission lines in the VUV region and it is more difficult to detect these elements in other spectral regions. Working in VUV region requires transmission of plasma radiation through the spectrograph to the VUV sensitive detector and the atmospheric absorption must be negligible all the way through the optical path. In paper I it was discovered that purging a conventional spectrograph and the optical path between the plasma plume and the slit of the spectrograph was enough to replace the air and prevent the atmospheric absorption. Also the potential of intensified charge-coupled device in VUV detection of the LIPS spectra was demonstrated. The capability of detect multiple emission lines simultaneously is a significant advantage, when measurements from a samples having a complicated matrix are carried out. With an ordinary ICCD equipped with UV grade quartz input window emission lines down to 165 nm could be detected. With an ICCD equipped with MgF₂ window emission lines of chlorine above 130 nm were measured.

The setup with quartz ICCD was used in analysis of sulfide minerals in the VUV region from drill core samples in paper II. It was demonstrated that rapid LIPS analysis could be used in mining industry for on-line sorting of the drill core samples for the further analysis. The potential of the experimental setup in identification of main minerals from drill core samples was reported and improvements for *in situ* work were suggested.

Brominated and chlorinated solid organic compounds were analyzed in paper III. It was observed, that the transmission efficiency of the spectrograph in the wavelengths below 150 nm is significantly lower. Also the atmospheric absorption was stronger and therefore a sample chamber with argon atmosphere was introduced. Because of the different matrices of the samples studied, internal standardization against carbon was used. A linear correlation between the halogen/carbon emission line intensity ratio and atomic ratios in the sample was verified. It was estimated, that compounds containing 90 carbon atoms against one bromine atom could be determined from analysis of bromine in VUV. For chlorine compounds the respective ratio was 20:1. It can be concluded, that the gas-purged setup for VUV presented in the thesis is most convenient at wavelengths above 165 nm. Thus ordinary ICCD could be used for the detection. If the sample chambers are needed below 165 nm, then proper vacuum chamber could be used, as well.

In the measurements of this thesis plasma was generated with excimer lasers operating at UV wavelengths. Short wavelengths of the excimer lasers offer high excitation energies and thus very efficient multiphoton ionization, when laser-induced plasma is initiated. High absorbance of the UV wavelengths in many materials leads to more efficient ablation at the sample provided that the plasma shielding caused by the absorption and scattering of the laser pulse to the plasma plume can be avoided. The shielding as a function of laser irradiance and the focusing conditions was studied in paper IV by using ArF and KrF excimer lasers, operating at 193 nm and 248 nm, respectively, to generate plasma in copper sample. Attenuation of the emission intensities was observed at irradiances above $\sim 1 \text{ GW cm}^{-2}$ regardless the delay time between the laser pulse and the detection. In argon atmosphere the shielding was increased, especially, when focal point was in front of the sample surface. The influence of the laser repetition rate on shielding in the range of 2-15 Hz was negligible. It can be concluded, that with ArF and KrF, irradiances below 1 GW cm^{-2} should be used for the optimal LIPS measurements, as the plasma shielding decreases the detected emission level.

REFERENCES

1. Y.-. Lee, K. Song and J. Sneddon: Laser induced plasmas for analytical atomic spectroscopy in *Lasers in analytical atomic spectroscopy* edited by J. Sneddon, T. L. Thiem and Y. -I Lee. VCH Publishers, Inc New York, **1997**, 197-235
2. D.A. Rusak, B.C. Castle, B.W. Smith and J.D. Winefordner, *TRAC Trend. Anal. Chem.* **17** (1998) 453-461
3. J. Sneddon and Y.-. Lee, *Anal.Lett.* **32** (1999) 2143-2162
4. M.Z. Martin, M.-. Cheng and R.C. Martin, *Aerosol Sci. Tech.* **31** (1999) 409-421
5. S.J. Hill, S. Chenery, J.B. Dawson, E.H. Evans, A. Fisher, W.J. Price, C.M.M. Smith, K.L. Sutton and J.F. Tyson, *J. Anal. Atom. Spectrom.* **15** (2000) 763-805
6. E. Tognoni, V. Palleschi, M. Corsi and G. Cristoforetti, *Spectrochim. Acta B* **57** (2002) 1115-1130
7. J.M. Vadillo and J.J. Laserna, *Spectrochim. Acta B* **59** (2004) 147-161
8. H.M. Solo-Gabriele, T.G. Townsend, D.W. Hahn, T.M. Moskal, N. Hosein, J. Jambeck and G. Jacobi, *Waste Manage.* **24** (2004) 413-424
9. L.G. Blevins, C.R. Shaddix, S.M. Sickafoose and P.M. Walsh, *Appl. Optics* **42** (2003) 6107-6118
10. M. Kurihara, K. Ikeda, Y. Izawa, Y. Deguchi and H. Tarui, *Appl. Optics* **42** (2003) 6159-6165
11. L. Peter, V. Sturm and R. Noll, *Appl. Optics* **42** (2003) 6199-6205
12. M. Stepputat and R. Noll, *Appl. Optics* **42** (2003) 6120-6220
13. J.M. Vadillo, P.L. García, S. Palanco, D. Romero, J.M. Baena and J.J. Laserna, *Analytical and Bioanalytical Chemistry* **375** (2003) 1144-1147
14. H. Fink, U. Panne and R. Niessner, *Anal.Chem.* **74** (2002) 4334-4342
15. L. Barrette and S. Turmel, *Spectrochim. Acta B* **56** (2001) 715-723
16. J.E. Carranza, B.T. Fisher, G.D. Yoder and D.W. Hahn, *Spectrochim. Acta B* **56** (2001) 851-864

17. S. Klein, T. Stratoudaki, V. Zafiropoulos, J. Hildenhagen, K. Dickmann and T. Lehmkuhl, *Appl. Phys. A - Mater.* **69** (1999) 441-444
18. R.E. Neuhauser, U. Panne, R. Niessner and P. Wilbring, *Fresen. J. Anal. Chem.* **364** (1999) 720-726
19. U. Panne, M. Clara, C. Haisch and R. Niessner, *Spectrochim. Acta B* **53** (1998) 1969-1981
20. I. Gobernado-Mitre, A.C. Prieto, V. Zafiropoulos, Y. Spetsidou and C. Fotakis, *Appl. Spectrosc.* **51** (1997) 1125-1129
21. R.E. Neuhauser, U. Panne, R. Niessner, G. Petrucci, P. Cavalli and N. Omenetto, *Anal.Chim.Acta* **346** (1997) 37-48
22. C. Carlhoff and S. Kirchhoff, *Laser and Optoelektronik* **23** (1991)
23. G.M. Weyl: Physics of laser-induced breakdown: an update in *Laser-induced plasmas and applications* edited by L. J. Radziemski and D. A. Cremers. Marcel Dekker, Inc New York, **1989**, 1-59
24. R.E. Russo, *Appl. Spectrosc.* **19** (1995) 14A-27A
25. R.G. Root: Modeling of post-breakdown phenomena in *Laser-induced plasmas and applications* edited by L. J. Radziemski and D. A. Cremers. Marcel Dekker, Inc New York, **1989**, 69-103
26. L. Moenke-Blankenburg: Laser ablation for sample introduction: principles and applications in *Lasers in analytical atomic spectroscopy* edited by J. Sneddon, T. L. Thiem and Y. -I Lee. VCH Publishers, Inc New York, **1997**, 125-196
27. K.H. Song and X. Xu, *Appl.Surf.Sci.* **127-129** (1998) 111-116
28. Y.W. Kim: Fundamentals of analysis of solids by laser-produced plasmas in *Laser-induced plasmas and applications* edited by L. J. Radziemski and D. A. Cremers. Marcel Dekker, Inc New York, **1989**, 327-346
29. R. Fabbro, E. Fabre, F. Amiranoff, C. Garban-Labaune, J. Virmont, M. Weinfeld and C.E. Max, *Physical Review A* **26** (1982) 2289-2292
30. C.J. Lorenzen, C. Carlhoff, U. Hahn and M. Jogwich, *J. Anal. Atom. Spectrom.* **7** (1992) 1029-1035
31. R. Wisburn, I. Schechter, H. Schröder and K.L. Kompa, *Anal.Chem.* **66** (1994) 2964-2975
32. K.J. Grant and G.L. Paul, *Appl. Spectrosc.* **44** (1990) 1349-1354

33. K. Niemax, *Fresen. J. Anal. Chem.* **370** (2001) 332-340
34. A.K. Knight, N.L. Scherbarth, D.A. Cremers and M.J. Ferris, *Appl. Spectrosc.* **54** (2000) 331-340
35. W. Sdorra, J. Brust and K. Niemax, *Mikrochim. Acta* **108** (1992) 1-10
36. D. Basting: *Excimer laser technology: laser sources, optics, systems and applications*. Lambda Physik AG Göttingen **2001**, 289
37. J. Sneddon, Y.-. Lee, X. Hou, J.X. Zhou and R.G. Michel: Lasers in *Lasers in analytical atomic spectroscopy* edited by J. Sneddon, T. L. Thiem and Y. -I Lee. VCH Publishers, Inc New York, **1997**, 41-81
38. X. Hou and B.T. Jones, *Microchem. J.* **66** (2000) 115-145
39. H.R. Griem: *Plasma spectroscopy*. McGraw-Hill New York **1964**
40. D.R. Keefer: Laser sustained plasmas in *Laser-induced plasmas and applications* edited by L. J. Radziemski and D. A. Cremers. Marcel Dekker, Inc New York, **1989**, 169-206
41. *CRC Handbook of Chemistry and Physics*. CRC Press Inc **1984**, E-192; E-318
42. Y.-. Lee, S.P. Sawan, T.L. Thiem, Y.-. Teng and J. Sneddon, *Appl. Spectrosc.* **46** (1992) 436-441
43. M. Eyett and D. Baeuerle, *Appl. Phys. Lett.* **51** (1987) 2054-2055
44. Y. Iida and E.S. Yeung, *Appl. Spectrosc.* **48** (1994) 945-949
45. J.A. Aguilera, C. Aragón and F. Penalba, *Appl. Surf. Sci.* **127-129** (1998) 309-314
46. L.M. Cabalin and J.J. Laserna, *Spectrochim. Acta B* **53** (1998) 723-730
47. J.M. Vadillo, C.C. Garcia, J.F. Alcantara and J.J. Laserna, *Spectrochim. Acta B* **60** (2005) 948-954
48. H. Häkkänen and J. Korppi-Tommola, *Appl. Spectrosc.* **49** (1995) 1721-1728
49. J.A. Aguilera and C. Aragon, *Spectrochim. Acta B* **59** (2004) 1861-1876
50. H. Keller-Rudek and G.K. Moortgat, Available: www.atmosphere.mpg.de/spectral-atlas-mainz [2005, 06/09]
51. M.A. Khater, P. van Kampen, J.T. Costello, J.P. Mosnier and E.T. Kennedy, *Laser Part. Beams* **33** (2000) 2252-2262

52. A. González, M. Ortiz and J. Campos, *Appl. Spectrosc.* **49** (1995) 1632-1635
53. V. Sturm, L. Peter and R. Noll, *Appl. Spectrosc.* **54** (2000) 1275-1278
54. M. Hemmerlin, R. Meilland, H. Falk, P. Wintjens and L. Paulard, *Spectrochim. Acta B* **56** (2001) 661-669
55. R. Noll, H. Bette, A. Brysch, M. Kraushaar, I. Monch, L. Peter and V. Sturm, *Spectrochim. Acta B* **56** (2001) 637-649
56. M.A. Khater, J.T. Costello and E.T. Kennedy, *Appl. Spectrosc.* **56** (2002) 970-982
57. V. Sturm, J. Vrenegor, R. Noll and M. Hemmerlin, *J.Anal.At.Spectrom.* **19** (2004) 451-456
58. C. Aragón, J.A. Aquilera and F. Penalba, *Appl. Spectrosc.* **53** (1999) 1259-1267
59. M.H. Núñez, P. Cavalli, G. Petrucci and N. Omenetto, *Appl. Spectrosc.* **54** (2000) 1805-1816
60. I. Radivojevic, R. Niessner, C. Haisch, S. Florek, H. Becker-Ross and U. Panne, *Spectrochim. Acta B* **59** (2004) 335-343
61. L. Radziemski, D.A. Cremers, K. Benelli, C. Khoo and R.D. Harris, *Spectrochim. Acta B* **60** (2005) 237-248
62. G.R. Carruthers: Ultraviolet spectroscopy in astronomy in *Ultraviolet spectroscopy and UV lasers* edited by P. Misra and M. A. Dubinskii. Marcel Dekker Inc. New York, USA, **2002**, 499-556
63. I. Radivojevic, C. Haisch, R. Niessner, S. Florek, H. Becker-Ross and U. Panne, *Anal.Chem.* **76** (2004) 1648-1656
64. M. Sabsabi, R. Heon and L. St-Onge, *Spectrochim. Acta B* **60** (2005) 1211-1216
65. *Instruction manual for Oriel Instaspec V.* **1996**
66. K.J. Grant, G.L. Paul and J.A. O'Neill, *Appl. Spectrosc.* **45** (1991) 701-705
67. T.L. Thiem and P.J. Wolf, *Microchem.J.* **50** (1994) 244-252
68. I.B. Gornushkin, A. Ruíz-Medina, J.M. Anzano, B.W. Smith and J.D. Winefordner, *J. Anal. Atom. Spectrom.* **15** (2000) 581-586
69. Q. Sun, M. Tran, B.W. Smith and J.D. Winefordner, *Anal.Chim.Acta* **413** (2000) 187-195

70. S. Rosenwasser, G. Asimellis, B. Bromley, R. Hazlett, J. Martin, T. Pearce and A. Zigler, *Spectrochim. Acta B* **56** (2001) 707-714
71. J.A. Bolger, *Appl. Spectrosc.* **54** (2000) 181-188
72. J.M. Vadillo, I. Vadillo, F. Carrasco and J.J. Laserna, *Fresen. J. Anal. Chem.* **361** (1998) 119-123
73. D. Kossakovski and J.L. Beauchamp, *Anal.Chem.* **72** (2000) 4731-3737
74. C. Fabre, M.-. Boiron, J. Dubessy, M. Cathelineau and D.A. Banks, *Chem.Geol.* **182** (2002) 249-264
75. M.-. Boiron, A. Moissette, M. Cathelineau, D. Banks, C. Monnin and J. Dubessy, *Chem.Geol.* **154** (1999) 179-192
76. M.O. Vieitez, J. Hedberg, O. Launila and L. Berg, *Spectrochim. Acta B* **60** (2005) 920-925
77. F. Colao, R. Fantoni, V. Lazic, A. Paolini, F. Fabbri, G.G. Ori, L. Marinangeli and A. Baliva, *Planet.Space Sci.* **52** (2004) 117-123
78. B. Salle, J. Lacour, E. Vors, P. Fichet, S. Maurice, D.A. Cremers and R.C. Wiens, *Spectrochim. Acta B* **59** (2004) 1413-1422
79. Z.A. Arp, D.A. Cremers, R.D. Harris, D.M. Oschwald, J. Parker Gary R. and D.M. Wayne, *Spectrochim. Acta B* **59** (2004) 987-999
80. D.A. Cremers and L.J. Radziemski, *Anal.Chem.* **55** (1983) 1252-1256
81. M. Casini, M.A. Harith, V. Palleschi, A. Salvetti, D.P. Singh and M. Vaselli, *Laser Part. Beams* **9** (1991) 633-639
82. C. Haisch, R. Niessner, O.I. Matveev, U. Panne and N. Omenetto, *Fresen. J. Anal. Chem.* **356** (1996) 21-26
83. L. Dudragne, P. Adam and J. Amouroux, *Appl. Spectrosc.* **52** (1998) 1321-1327
84. L.M. Berman and P.J. Wolf, *Appl. Spectrosc.* **52** (1998) 438-443
85. M. Pardede, H. Kurniawan, M.O. Tjia, K. Ikezawa, T. Maruyama and K. Kagawa, *Appl. Spectrosc.* **55** (2001) 1229-1236
86. R. Sattmann, I. Mönch, H. Krause, R. Noll, S. Couris, A. Hatziapostolou, A. Mavromanolakis, C. Fotakis, E. Larrauri and R. Miguel, *Appl. Spectrosc.* **52** (1998) 456-461
87. M. Tran, Q. Sun, B.W. Smith and J.D. Winefordner, *Appl. Spectrosc.* **55** (2001) 739-744

88. G. Asimellis, S. Hamilton, A. Giannoudakos and M. Kompitsas, *Spectrochim. Acta B* **60** (2005) 1132-1139
89. L. St-Onge, E. Kwong, M. Sabsabi and E.B. Vadas, *Spectrochim. Acta B* **57** (2002) 1131-1140
90. U. Panne, R.E. Neuhauser, M. Theisen, H. Fink and R. Niessner, *Spectrochim. Acta B* **56** (2001) 839-850
91. D. Menut, P. Fichet, J.L. Lacour, A. Rivoallan and P. Mauchien, *Appl. Optics* **42** (2003) 6063-6071
92. V. Sturm and R. Noll, *Appl. Optics* **42** (2003) 6221-6225
93. O. Samek, D.C.S. Beddows, H.H. Telle, J. Kaiser, M. Liska, J.O. Caceres and U. Gonzalez, *Spectrochim. Acta B* **56** (2001) 865-875

PAPER I

Reproduced with permission from "Laser-induced plasma spectroscopy to as low as 130 nm when a gas-purged spectrograph and ICCD detection are used"
Kaski S., Häkkänen H., Korppi-Tommola J. *Applied Optics*, 2003, 42, 6036-6039
© 2003 Optical Society of America

<https://doi.org/10.1364/AO.42.006036>

PAPER II

Reproduced with permission from "Sulfide mineral identification using laser-induced plasma spectroscopy" Kaski S., Häkkänen H., Korppi-Tommola J. *Minerals Engineering*, 2003, 16, 1239-1243
© 2003 Elsevier Ltd.

<https://doi.org/10.1016/j.mineng.2003.05.001>

PAPER III

Reproduced with permission from "Determination of Cl/C and Br/C ratios in pure organic solids using laser-induced plasma spectroscopy in near vacuum ultraviolet" Kaski S., Häkkänen H., Korppi-Tommola J. *Journal of Analytical Atomic Spectrometry*, **2004**, 19, 474-478

© 2004 The Royal Society of Chemistry

<https://doi.org/10.1039/B315410F>

PAPER IV

Reproduced with permission from "A spectroscopic study of shielding in plasmas generated by excimer laser radiation" Kaski S., Häkkänen H., Korppi-Tommola J. *Analytical and Bioanalytical Chemistry*, submitted for publication. Unpublished work © 2005 Springer Verlag

A SPECTROSCOPIC STUDY OF SHIELDING IN PLASMAS GENERATED BY EXCIMER LASER RADIATION

Saara Kaski*, Heikki Häkkänen and Jouko Korppi-Tommola
Department of Chemistry, P.O. BOX 35, FIN-40014 University of Jyväskylä,
FINLAND

*E-mail for correspondence: saara.kaski@ju.fi

Abstract:

Plasma shielding effect in UV plasma generation and its influence on laser-induced plasma spectroscopy (LIPS) analysis was studied. Irradiance values on a pure copper surface were changed by adjusting the focusing lens-to-sample distance. Effects of focusing on plasma shielding in front of and behind the sample surface were studied. Both ArF and KrF lasers were used to generate plasmas, and irradiances at the sample varied in the range of 0.02 - 4 GW cm⁻². Plasma shielding effect was observed for both lasers at irradiances larger than 1 GW cm⁻², even at longer time delays between the laser pulse and the detection. In general, focusing in front of the sample produced higher emission line intensities than focusing at the same distance behind the sample surface. Shielding effect was somewhat stronger in argon flow than in air. Influence of laser repetition rate on plasma shielding was negligible. Plasma threshold value for copper was estimated to be about 0.1 GW cm⁻².

keywords: laser-induced plasma spectroscopy; LIPS; laser-induced breakdown spectroscopy; LIBS; plasma shielding; copper; excimer laser

INTRODUCTION

When high-power laser light irradiates material, most of the radiation is reflected from the surface and only a fraction is absorbed. Threshold irradiances to initiate the plasma are typically 10^8 - 10^9 W cm⁻², depending on the sample, but irradiances as low as 10^6 W cm⁻² have been used in plasma generation.¹ During the energy transfer to the material, the local surface temperature rises nearly instantaneously and surface vaporization begins. Rapidly in the layers below the surface, the thermal energy exceeds the energy of vaporization of the material, resulting in laser ablation *i.e.* explosion of the surface material and to plasma formation.¹⁻⁵ Plasma generation mechanism is dependent on the laser wavelength: the electron density growth in the plasma at wavelengths > 1000 nm is mainly due to the electron – neutral collisions resulting in inverse bremsstrahlung (IB), while at UV wavelengths it is dominated by the photoionization processes.^{1,4}

Nanosecond laser pulse interacts with an expanding plasma plume. For example for the plasma generated with KrF laser at irradiances from 0.08 to 0.4 GW/cm², the average plume velocities of 2 – 8 μm/ns have been measured.⁶ At high laser irradiances, when the plume interacts with the incoming radiation, it produces a partially ionized plasma that strongly absorbs/scatters laser light and blocks the target from the subsequent exposure to the laser radiation, considerably reducing the ablation efficiency. This effect is called plasma shielding. In cases where laser energy is absorbed to the plasma through IB processes, the electron cascade growth rate is proportional to λ^3 .¹ Thus the influence of the plasma shielding is expected to be reduced, when short wavelengths are used for plasma generation. However, as the absorption probability through IB is highly dependent on the electron concentration of the plasma, its importance may increase during the ablation via photoionization processes that produce high electron concentrations.⁷ During the laser ablation also small particles are generated in the plume and scattering of UV wavelengths will take place. As the intensity of scattered light is proportional to λ^4 , this effect becomes important at short laser wavelengths.

Plasma shielding has been studied by measuring directly the attenuated energy via a small hole in the sample material using different KrF (248 nm) excimer laser fluences. It was observed that at the irradiances of ~ 0.2 GW cm⁻², less than 45 % of the initial laser pulse energy reached the sample surface.⁸ Plasma shielding thresholds

have also been estimated by measuring the temporal profiles of the reflected and/or transmitted laser pulse, because the plasma shielding changes the pulse profile. In such analysis with KrF laser generated plasmas, the shielding was observed at irradiance of around 0.3 GW cm^{-2} in several samples.⁹ With XeCl (308 nm) laser pulses as low as 0.05 GW cm^{-2} threshold for $\text{YBa}_2\text{Cu}_3\text{O}_7$ sample has been reported.^{10,11} In silicon carbide the shielding threshold was greater than 0.12 GW cm^{-2} for pulses of KrF laser.¹² The variation in the reported shielding threshold values may be due to the sample properties, but also due to the different experimental conditions.

Laser-induced plasma spectroscopy (LIPS), described in several review articles,^{3,5,13} utilizes direct optical emission from atoms and ions of the plasma for the elemental analysis of the sample. In LIPS experiments the plasma shielding is observed as a saturation of the emission line intensity as a function of laser irradiance. Laser irradiance is inversely proportional to the spot size of the beam at the sample and the pulse duration and directly proportional to the pulse energy. The influence of the focusing in LIPS measurements has been previously studied for laser wavelengths in the NIR and visible.¹⁴⁻¹⁸ At high irradiances at these wavelengths focusing in front of the sample generates an air plasma and therefore focusing at negative lens-to-sample distances (LTSD) is preferred *i.e.* the laser beam is focused behind the sample surface. However, at irradiances below the breakdown threshold of air the Multari *et al.*¹⁴ showed, that ablation rates and emission intensity ratios were approximately the same, independent of whether the focus was in front or behind the material surface. Bulatov *et al.*¹⁵ obtained in their imaging studies, the strongest intensities, when the laser beam was focused in front of the sample. On the other hand, in the study of spatial distribution of emission line intensities and plasma parameters by Aguilera *et al.*¹⁸ the optimal focal conditions were found, when the beam was focused behind the sample surface. In their study, with increasing pulse energy the maximum emission intensity was obtained by moving the focus deeper inside the sample.

The LIPS signal is also dependent on laser wavelength used to generate plasmas. In metal samples the saturation of line intensities occurs at lower laser irradiances for the fundamental of Nd:YAG laser at 1064 nm than for the second harmonic wavelength at 532 nm, for example in copper at 2.64 GW cm^{-2} and $>8 \text{ GW cm}^{-2}$, respectively.¹⁹ However, in this study the spot size was ~ 4 times larger in case of the fundamental than for the second harmonic beam, which may partly explain the different saturation values. Plasma shielding has been reported to be stronger with

larger spot sizes than with smaller spot sizes, which has been related to the physical size of the plasma plume.^{8,20}

In the present work, in addition to varying the position of the focus of the laser beam with respect to the sample surface, measurements at several laser pulse energies were carried out. Irradiances at the sample were in range of 0.02 - 4 GW cm⁻². Plasma shielding of ArF and KrF excimer laser pulses was studied by measuring LIPS spectra of a pure copper sample. Also influences of argon atmosphere and laser repetition rate on plasma shielding were studied.

EXPERIMENTAL

The experimental setup is presented in Fig. 1. Plasma was produced either by using ArF excimer laser (Optex, Lambda Physik) operating at 193 nm with pulse duration of 8 ns (FWHM) or KrF excimer laser (Optex, Lambda Physik) operating at 248 nm with pulse duration of 9 ns (FWHM). Pulse durations were determined with a Tektronix TDS 2002 oscilloscope and a fast DET 200 photodiode. The optical setup was kept fixed in all experiments and only the lasers were interchanged.

A circular aperture with a diameter of 3 mm was used to select the central part of the 4 x 7 mm laser beam. For the focusing a UV-grade fused silica 40-mm planoconvex lens was used. Pulse energies at the sample were measured with an energy meter (Ophir Optronics Ltd.) and they were adjusted with an optical attenuator. Pulse energies of the ArF laser at the sample ranged from 0.01 to 0.9 mJ and pulse energies of the KrF laser from 0.01 to 1.6 mJ. The relative standard deviation of the pulse to pulse energy fluctuations were about 1.2 % for the ArF and 2.8 % for the KrF laser. The spot size at the sample was varied by changing the position of the focusing lens with respect to the sample surface. Lens-to-sample distance was varied with 0.2 mm steps by using a translational stage. Spot sizes were determined with a microscope by measuring the diameters of the holes ablated in coated paper with 100 laser pulses at each LTSD. Smallest spot size created in paper with ArF pulses was 0.3×10^{-4} cm² and with KrF laser pulses 0.6×10^{-4} cm². Errors in the spot size determinations were estimated to be of the order of 0.1×10^{-4} cm². Laser irradiances at the sample were calculated from the determined spot sizes and measured pulse energies.

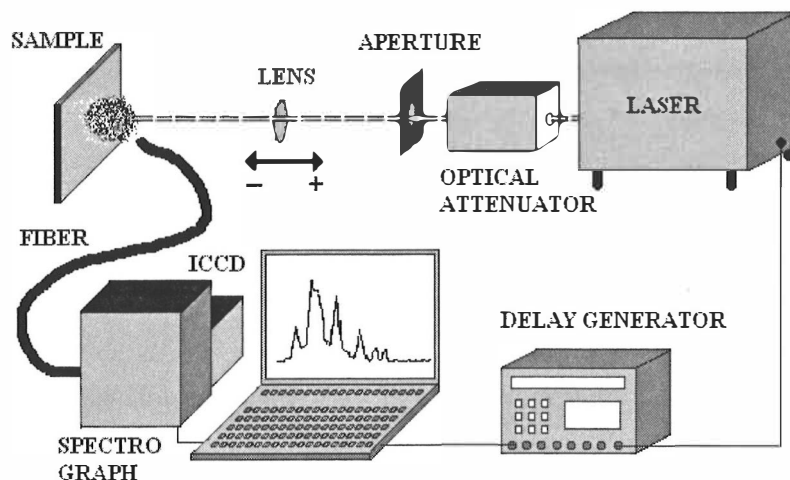


Figure 1: Experimental setup

A 150-mm Czerny-Turner spectrograph (Acton Research Corporation, SP-150) used in the experiments had a grating with $600 \text{ grooves mm}^{-1}$. Plasma emission was collected to the slit of the spectrograph with the aid of an optical fiber bundle (Oplatek Oy) manufactured of UV grade fused silica. The fiber was at ~ 45 degrees angle from the plasma axis. The slit width used was $\sim 150 \text{ }\mu\text{m}$ and a cutoff filter at 435 nm was used to prevent the appearance of the 2nd order lines in the spectra. The resolution of the spectrograph was about 0.8 nm in the spectral region used. Emission was detected with an ICCD detector (Oriel, Instaspec V) having a 1024×256 pixel imaging area and a 18 mm diameter intensifier. A delay generator (Stanford Research System, Inc., DG 535) was used to set the delay time, which were 100 ns in most measurements. The measurement gate width was 100 ns.

Pure copper (Cu 99.999%) was used as a sample in the measurements. The copper surface was mechanically polished to remove the dark oxide layer. In addition 20 cleaning pulses were used at each measurement point before spectra were recorded. To increase signal-to-noise ratio, spectra were averaged from 20 laser pulses. The error bars describing the intensity variations in the measurements were estimated from 5 such spectra measured at a each lens-to-sample distance. The repetition rate in the measurements was mainly 15 Hz. Non-resonance copper emission lines were recorded in the range from 430 to 560 nm to avoid self-absorption. The influence of atmosphere was investigated with argon gas flowing towards plasma.

RESULTS AND DISCUSSION

The focal point of ArF laser beam was closer to the focusing lens than that of the KrF laser beam. The focal distances given in the figures below have been measured from the true focal point. Negative and positive values indicate focusing inside and in front of the sample, respectively. Visually breakdown of air was not observed.

Intensity profiles of background corrected copper emission lines as a function of LTSD are presented in Fig. 2. Although the pulse energies of both lasers were adjusted to the same level, the maximum irradiance for ArF laser pulses was 4.0 GW cm^{-2} , while that for the KrF laser was pulses 1.7 GW cm^{-2} . This difference is a result of a smaller spot size of the ArF laser beam at the focus. In the focal area the irradiance is highest, but the emission intensity is attenuated because of the shielding. A lot stronger shielding is observed in the profiles for ArF laser due to the higher irradiance values, but influence of the shielding is similar in all emission lines in the plasma generated with a same laser. Therefore the dependencies of the line intensities on focusing distance are presented in the following only for the strongest copper emission peak in at $\sim 522 \text{ nm}$ and consisting of lines at 521.8 and 522.0 nm .

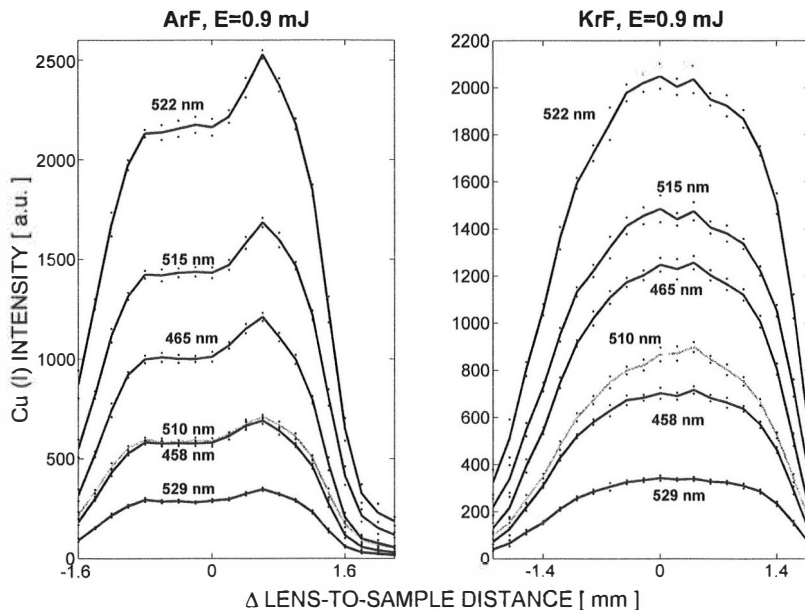
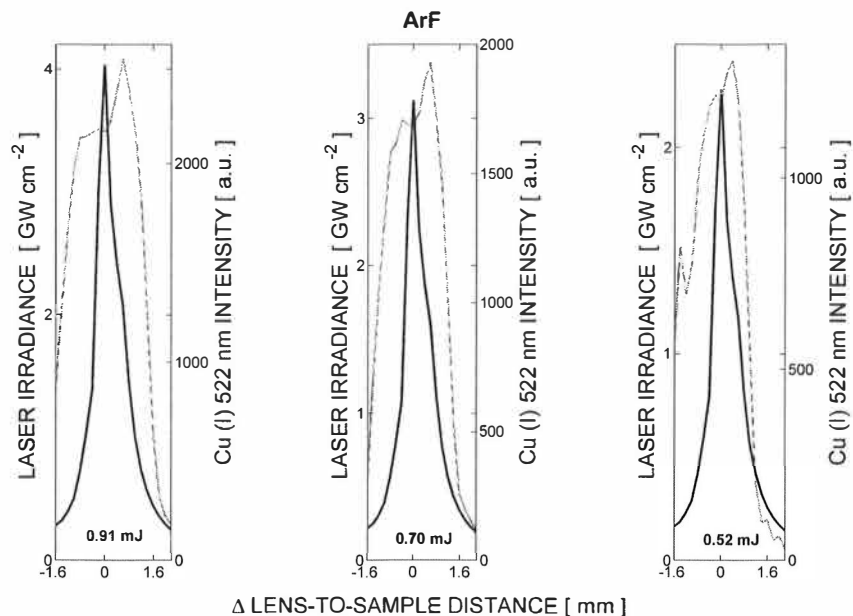


Figure 2: Intensities of background corrected copper line as a function of LTSD. The errors are estimated as a standard deviation of 5 measurements. The delay and the gate times were 100 ns.

The emission intensity profiles at several laser energies are plotted against the laser irradiance in Figs. 3 i and ii. The shielding can be still observed at 0.26 mJ pulse energy *i.e.* maximum irradiance above 1.1 GW cm^{-2} at the sample. In the profiles obtained for KrF laser pulses the shielding is as well present at irradiances of about 1 GW cm^{-2} (Fig. 4), but not at irradiances below this threshold value. The width of the intensity profile as a function of LTSD is decreased, when the laser pulse energy is reduced (Figs. 3 and 4). When the pulse energy is decreased, the intensity maximum of the profile shifts towards the focal point in both lasers. A dip in the intensity profile obtained for KrF laser can be observed at the high pulse energies, when the focus is in front of the sample. A possible reason for this could be breakdown of air, although the irradiances are lower than in the ArF laser beam focus.

With high irradiances from ArF laser, the maximum intensity is obtained, when focal plane is in front of the sample. Analysis of the ablation craters generated in coated paper (used for estimation of focal spot sizes) showed that the bottom of the crater is not as flat at negative LTSD's as for positive LTSD's. This is most likely due to the difference in focal length of the rays reaching focal area near and far from the optical axis caused by the spherical aberration of the lens. Such an effect may result in somewhat higher irradiance at the center of the laser beam and thus increased shielding at negative LTSD values.



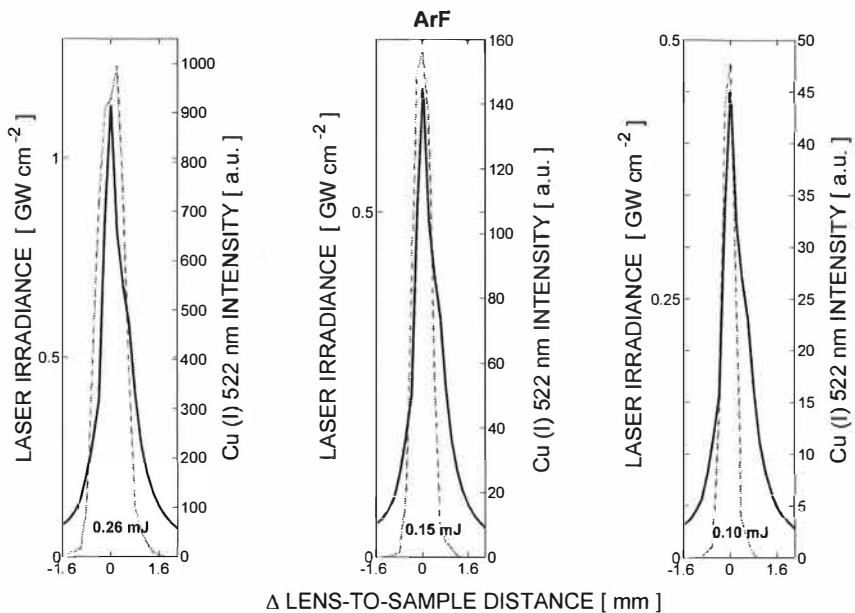


Figure 3: Intensity profiles of the copper 522 nm emission peak (gray) and the calculated laser irradiance at the sample (black) as a function of the lens-to-sample distance for ArF laser at (i) high pulse energies and (ii) small pulse energies. The delay and the gate times were 100 ns. The dip in (i) at 0.52 mJ in the LTSD=-1.4 is an artifact.

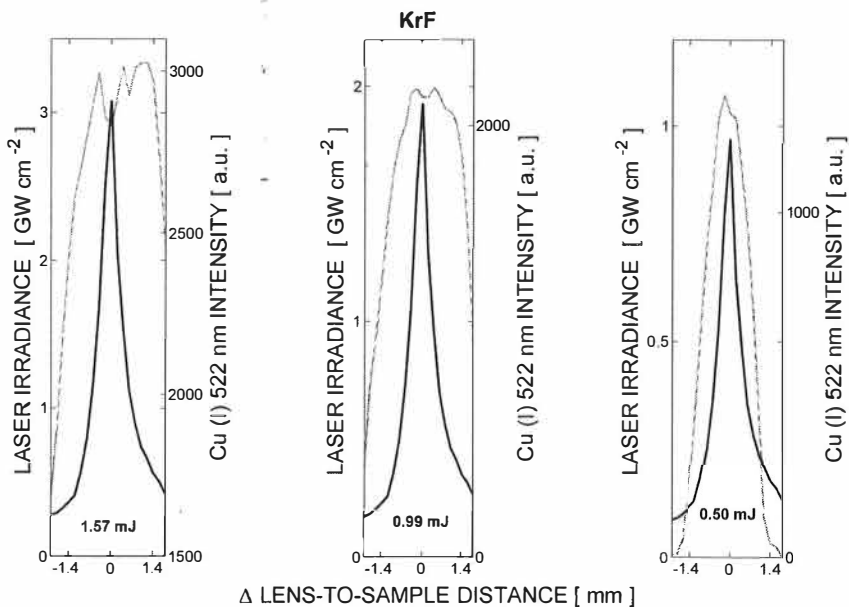


Figure 4: Intensity profiles of the copper (gray) and the calculated laser irradiance at the sample (black) as a function of the lens-to-sample distance.

According to the profile measurements, the plasma threshold irradiance for both lasers in copper is of the order of 0.1 GW cm^{-2} , which it is comparable with the plasma threshold irradiance, approximately 0.3 GW cm^{-2} determined with Nd:YAG at 532 nm LIPS measurements for the same material in other studies.^{19,21} The plasma threshold somewhat depends on laser wavelength, because material absorption coefficients are wavelength dependent.

However, the plasma threshold is also dependent on LTSD (Fig. 5). The plasma shielding can be observed when the emission intensity tapers off as a function of the irradiance. At the focal point the saturation is observed at somewhat higher irradiances, which is most likely caused by stronger shielding with larger spot sizes. When the threshold irradiance is approached, the background corrected emission intensity curves towards zero. The plasma threshold seems to be lowest at positive LTSD and the highest at the focal point. The focusing parameters seem to have an influence on plasma threshold and hence estimations obtained from LIPS measurements presenting intensity against irradiance have to be considered with caution.

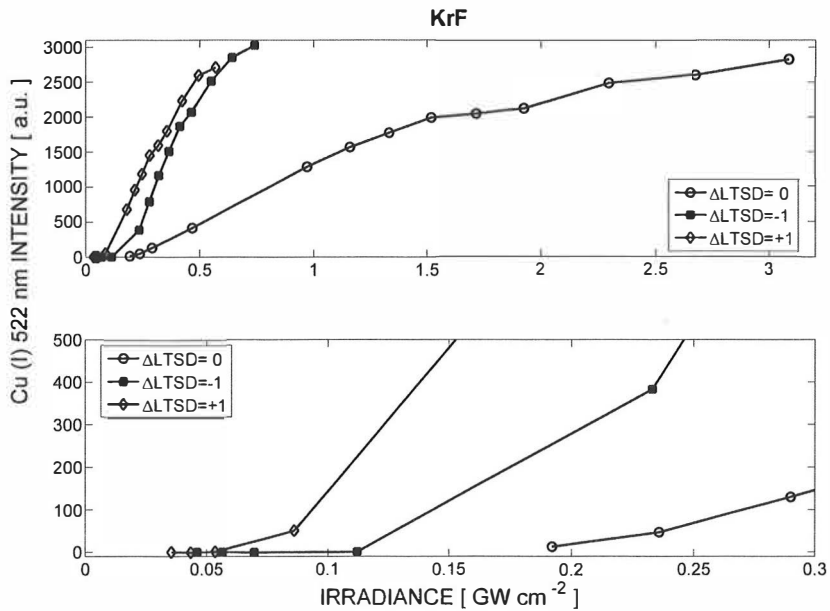


Figure 5: The behavior of copper intensity at different LTSD as a function of irradiance for KrF laser. The influence of the plasma shielding can be observed at higher irradiances.

The influence of the delay time between the laser pulse and the measurement on shielding observed at high irradiances was studied for both lasers. As illustrated in the profiles of Fig. 6 for the ArF laser, the dip caused by the shielding in the region of the focal plane can still be observed after 800 ns delay. The profile, however, is narrower at the longer delay times. The plasma emission lifetime depends on the laser pulse irradiance and it has been observed previously, that the decay of the line intensities is faster at low than at high irradiances.²² At longer delay times the intensity from the larger spot sizes has decayed to lower levels than intensity for smaller spot sizes near the focal area and therefore rather short delays were used through the study.

The decay of the copper emission line intensity was faster in plasmas generated by ArF laser pulses (Fig. 7 i) at a same irradiance, although the shielding behavior was similar for both lasers. Also the intensities of the ionic lines of around 490 nm were higher in KrF laser generated plasmas, indicating higher plasma temperature (Fig. 7 ii). In these experiments both lasers had a spot size of $\sim 2 \times 10^{-4} \text{ cm}^2$ and the pulse energy was $\sim 0.8 \text{ mJ}$, giving the irradiance well below the observed shielding threshold limit. Lower plasma temperature of ArF laser generated plasmas may be a result of more efficient scattering of ArF laser photons than KrF photons from the plasma. Plasma heating via IB can be stronger at 248 nm than at 193 nm which would also result in slower decay of the KrF generated signal. Different absorption coefficients of copper at plasma generation wavelengths could induce different initial plasma temperatures and varying decay profiles, as well.

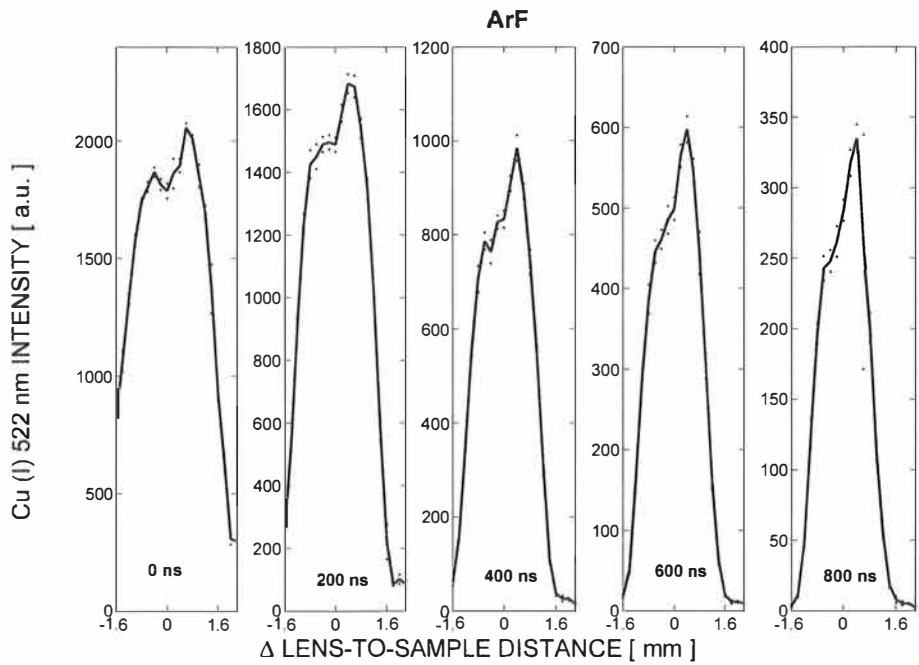
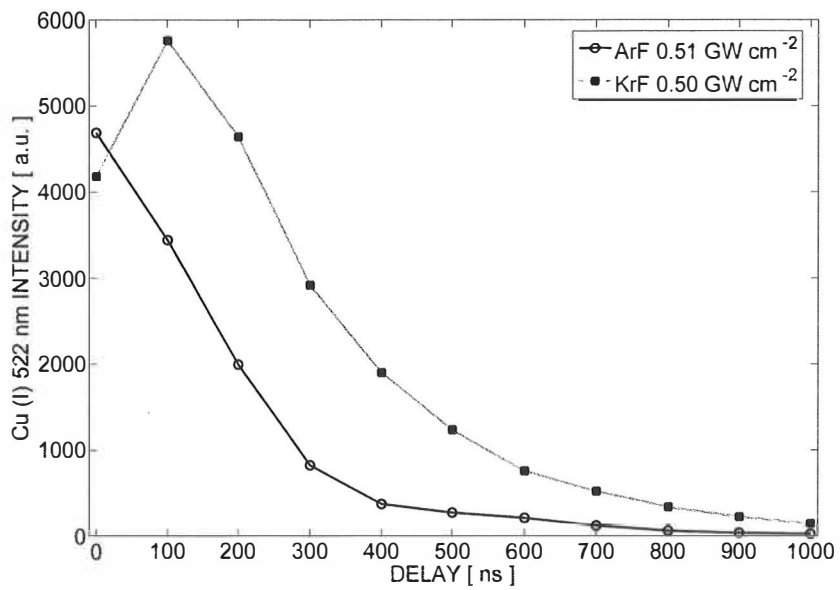


Figure 6: Influence of the measurement delay to the copper emission line intensity profile at the energy of 0.8 mJ. The measurement gate was 100 ns.



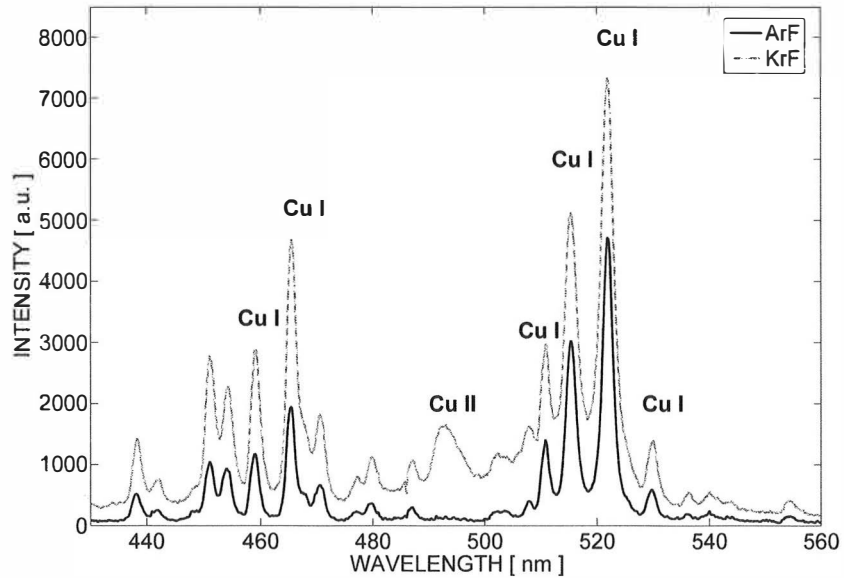


Figure 7:(i) Intensity of copper atomic line as a function of delay time. Measurement gate was 100 ns. (ii) The LIPS spectra of copper measured at irradiance of $\sim 0.5 \text{ GW cm}^{-2}$ at the delay time of 100 ns show the largest difference in emission line intensities, when ArF and KrF laser pulses were used to generate plasmas.

The results described above were obtained at laser repetition rate of 15 Hz. Although the plasma lifetime at the low energies used in the study is a lot shorter than the time delay between the consecutive laser pulses, at higher repetition rates there is a possibility that some small particles from the previous ablation process are still present and cause scattering and absorption of the next incoming laser pulse. Plasma from such particles flying above the sample surface may be generated and then the amount of energy left for ablation of the sample would be reduced. To study such a possibility the copper emission line intensity profiles at different LTSD's were recorded by using low repetition rates at fixed pulse energies (0.8 mJ) for both lasers (Fig. 8). Using repetition rates from 2 to 15 Hz did not show significant changes of the line intensities at different LTSD's and small deviation of the profiles at different repetition rates is seen only near the focal plane, where the irradiance is highest.

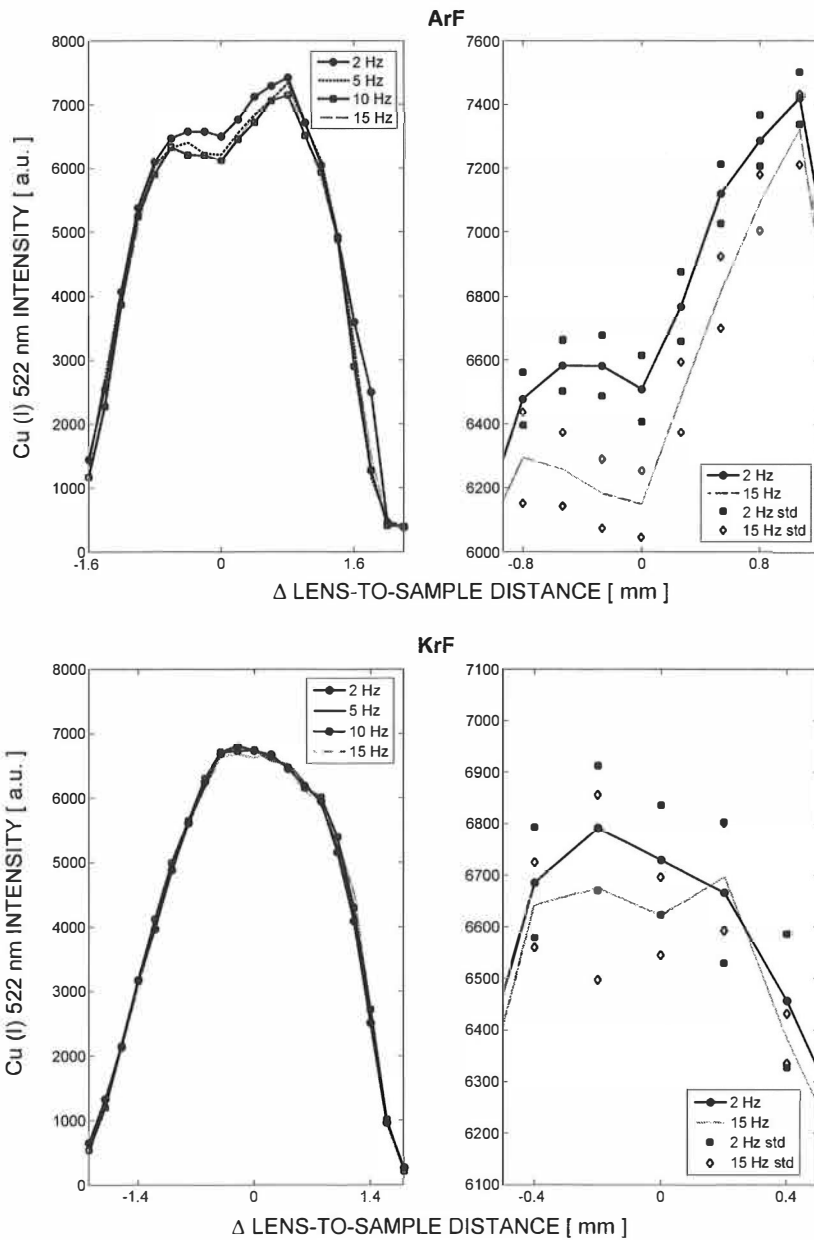


Figure 8: Influence of the repetition rate to the copper emission line intensity profile for (i) ArF and (ii) KrF laser generated plasmas. The measurement delay and the gate were 100 ns.

Argon is often used as a buffer gas in LIPS measurements to obtain higher emission line intensities due to the slower expansion and cooling of the plasma. Argon is also ionized and excited in the plasma and may serve as a reservoir of the laser energy in the ablation process. On the other hand, the inverse bremsstrahlung has been observed to be enhanced in argon.²³ Breakdown of argon near the main plasma at different focusing distances of Nd:YAG laser has been demonstrated by Aguilera *et al.*,¹⁸ leading to increased shielding.

Dependence of copper emission line intensities and shielding in UV laser generated plasma at various LTSD's under argon atmosphere is demonstrated in Fig. 9. The intensity profile is wider in argon atmosphere than in air. This is most likely due to the different temporal behavior of the emission intensity in argon and air because of higher plasma temperature in argon. That the dip caused by the attenuation of the emission intensities wider in argon than in air indicates stronger plasma shielding in argon, especially at positive LTSD values. This could be understood as breakdown of the argon buffer when the laser beam is focused in front of the sample. Nevertheless, the value of the shielding threshold in argon was similar to that observed from the measurements in air.

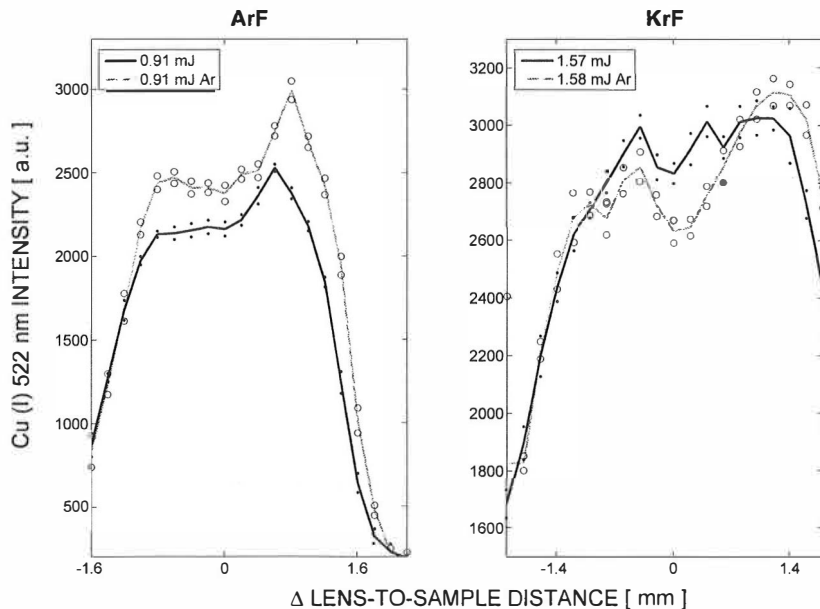


Figure 9: Influence of argon atmosphere on the emission intensity profile of copper peak at 522 nm (gray) for ArF and KrF laser generated plasmas when compared to the profile measured in air (black). Maximum irradiancies were ~ 4 and ~ 3 GW cm^{-2} for ArF and KrF, respectively. The measurement delay and the gate width were 100 ns.

CONCLUSIONS

Shielding in UV laser generated plasma was studied by using laser-induced plasma spectroscopy. Plasma shielding was observed at irradiances exceeding $\sim 1 \text{ GW cm}^{-2}$ for both ArF and KrF excimer lasers pulses. Emission intensity profiles at varying lens-to-sample distances from a pure copper showed attenuation of the emission intensity on both sides of the focal plane where the irradiance is highest. Thus to obtain maximum emission intensity in LIPS experiments one has to minimize the effects of shielding by optimizing focusing of the laser on the sample surface. According to the results of the present study of UV generated plasmas, highest intensities are obtained, when the focal plane of the laser beam is in front of the sample surface. The plasma shielding remained also at longer delay times. The laser repetition rate did not significantly affect to the plasma shielding. In argon atmosphere the shielding was somewhat stronger than in air, especially when the laser beam was focused in front of the sample.

REFERENCES

1. G.M. Weyl: Physics of laser-induced breakdown: an update in *Laser-induced plasmas and applications* edited by L. J. Radziemski and D. A. Cremers. Marcel Dekker, Inc New York, **1989**, 1-59
2. R.E. Russo, *Appl. Spectrosc.* **19** (1995) 14A-27A
3. L. Moenke-Blankenburg: Laser ablation for sample introduction: principles and applications in *Lasers in analytical atomic spectroscopy* edited by J. Sneddon, T. L. Thiem and Y. -I Lee. VCH Publishers, Inc New York, **1997**, 125-196
4. Y.-. Lee, K. Song and J. Sneddon: Laser induced plasmas for analytical atomic spectroscopy in *Lasers in analytical atomic spectroscopy* edited by J. Sneddon, T. L. Thiem and Y. -I Lee. VCH Publishers, Inc New York, **1997**, 197-235
5. K. Niemax, *Fresen. J. Anal. Chem.* **370** (2001) 332-340
6. K.H. Song and X. Xu, *Appl.Surf.Sci.* **127-129** (1998) 111-116
7. R.G. Root: Modeling of post-breakdown phenomena in *Laser-induced plasmas and applications* edited by L. J. Radziemski and D. A. Cremers. Marcel Dekker, Inc New York, **1989**, 69-103
8. H. Schmidt, J. Ihlemann, B. Wolff-Rottke, K. Luther and J. Troe, *J.Appl.Phys.* **83** (1998) 5458-5468

- [32] Kuokkanen, Tauno: Chlorocymenes and Chlorocymenenes: Persistent chlorocompounds in spent bleach liquors of kraft pulp mills. (40 pp.) 1989
- [33] Mäkelä, Reijo: ESR, ENDOR, and TRIPLE resonance study on substituted 9,10-anthraquinone radicals in solution. (35 pp.) 1990
- [34] Veijanen, Anja: An integrated sensory and analytical method for identification of off-flavour compounds. (70 pp.) 1990
- [35] Kasa, Seppo: EPR, ENDOR, and TRIPLE resonance and molecular orbital studies on a substitution reaction of anthracene induced by thallium(III) in two fluorinated carboxylic acids. (114 pp.) 1990
- [36] Herve, Sirpa: Mussel incubation method for monitoring organochlorine compounds in freshwater recipients of pulp and paper industry. (145 pp.) 1991
- [37] Pohjola, Pekka: The electron paramagnetic resonance method for characterization of Finnish peat types and iron(III) complexes in the process of peat decomposition. (77 pp.) 1991
- [38] Paasivirta, Jaakko (Ed.): Organochlorines from Pulp Mills and Other Sources. Research Methodology Studies 1988–91. (120 pp.) 1992
- [39] Veijanen, Anja (Ed.): VI National Symposium on Mass Spectrometry, May 13–15, 1992, Abstracts. (55 pp.) 1992
- [40] Rissanen, Kari (Ed.): The 7th National Symposium on Inorganic and Analytical Chemistry, May 22, 1992, Abstracts and Program. (153 pp.) 1992
- [41] Paasivirta, Jaakko (Ed.): CEOEC'92, Second Finnish-Russian Seminar: Chemistry and Ecology of Organo-Element Compounds. (93 pp.) 1992
- [42] Koistinen, Jaana: Persistent polychloroaromatic compounds in the environment: structure-specific analyses. (50 pp.) 1993
- [43] Virkki, Liisa: Structural characterization of chlorolignins by spectroscopic and liquid chromatographic methods and a comparison with humic substances. (62 pp.) 1993
- [44] Helenius, Vesa: Electronic and vibrational excitations in some biologically relevant molecules. (30 pp.) 1993
- [45] Leppä-aho, Jaakko: Thermal behaviour, infrared spectra, and X-ray structures of some new rare earth chromates(VI). (64 pp.) 1994
- [46] Kotila, Sirpa: Synthesis, structure, and thermal behavior of solid copper(II) complexes of 2-amino-2-hydroxymethyl-1,3-propanediol. (111 pp.) 1994
- [47] Mikkonen, Anneli: Retention of molybdenum(VI), vanadium(V), and tungsten(VI) by kaolin and three Finnish mineral soils. (90 pp.) 1995
- [48] Suontamo, Reijo: Molecular orbital studies of small molecules containing sulfur and selenium. (42 pp.) 1995
- [49] Hämäläinen, Jouni: Effect of fuel composition on the conversion of fuel-N to nitrogen oxides in the combustion of small single particles. (50 pp.) 1995
- [50] Nevalainen, Tapio: Polychlorinated diphenyl ethers: synthesis, NMR spectroscopy, structural properties, and estimated toxicity. (76 pp.) 1995
- [51] Aittola, Jussi-Pekka: Organochloro compounds in the stack emission. (35 pp.) 1995
- [52] Harju, Timo: Ultrafast polar molecular photophysics of (dibenzylmethine)borondifluoride and 4-aminophthalimide in solution. (61 pp.) 1995
- [53] Maatela, Paula: Determination of organically bound chlorine in industrial and environmental samples. (83 pp.) 1995
- [54] Paasivirta, Jaakko (Ed.): CEOEC'95, Third Finnish-Russian Seminar: Chemistry and Ecology of Organo-Element Compounds. (109 pp.) 1995
- [55] Huuskonen, Juhani: Synthesis and structural studies of some supramolecular compounds. (54 pp.) 1995
- [56] Palm, Helena: Fate of chlorophenols and their derivatives in sawmill soil and pulp mill recipient environments. (52 pp.) 1995
- [57] Rantio, Tiina: Chlorohydrocarbons in pulp mill effluents and their fate in the environment. (89 pp.) 1997
- [58] Ratilaincn, Jari: Covalent and non-covalent interactions in molecular recognition. (37 pp.) 1997
- [59] Kolehmainen, Erkki (Ed.): XIX National NMR Symposium, June 4–6, 1997, Abstracts. (89 pp.) 1997
- [60] Matilainen, Rose: Development of methods for fertilizer analysis by inductively coupled plasma atomic emission spectrometry. (41 pp.) 1997

- [61] Koistinen, Jari (Ed.): Spring Meeting on the Division of Synthetic Chemistry, May 15–16, 1997, Program and Abstracts. (36 pp.) 1997
- [62] Lappalainen, Kari: Monomeric and cyclic bile acid derivatives: syntheses, NMR spectroscopy, and molecular recognition properties. (50 pp.) 1997
- [63] Laitinen, Eira: Molecular dynamics of cyanine dyes and phthalimides in solution: picosecond laser studies. (62 pp.) 1997
- [64] Eloranta, Jussi: Experimental and theoretical studies on some quinone and quinol radicals. (40 pp.) 1997
- [65] Oksanen, Jari: Spectroscopic characterization of some monomeric and aggregated chlorophylls. (43 pp.) 1998
- [66] Häkkänen, Heikki: Development of a method based on laser-induced plasma spectrometry for rapid spatial analysis of material distributions in paper coatings. (60 pp.) 1998
- [67] Virtapohja, Janne: Fate of chelating agents used in the pulp and paper industries. (58 pp.) 1998
- [68] Airola, Karri: X-ray structural studies of supramolecular and organic compounds. (39 pp.) 1998
- [69] Hyötyläinen, Juha: Transport of lignin-type compounds in the receiving waters of pulp mills. (40 pp.) 1999
- [70] Ristolainen, Matti: Analysis of the organic material dissolved during totally chlorine-free bleaching. (40 pp.) 1999
- [71] Eklun, Tero: Development of analytical procedures with industrial samples for atomic emission and atomic absorption spectrometry. (43 pp.) 1999
- [72] Väliisaari, Jouni: Hygiene properties of resol-type phenolic resin laminates. (129 pp.) 1999
- [73] Hu, Jiwei: Persistent polyhalogenated diphenyl ethers: model compounds syntheses, characterization, and molecular orbital studies. (59 pp.) 1999
- [74] Malkavaara, Petteri: Chemometric adaptations in wood processing chemistry. (56 pp.) 2000
- [75] Kujala Elena, Laihia Katri, Nieminen Kari (Eds.): NBC 2000, Symposium on Nuclear, Biological, and Chemical Threats in the 21st Century. (299 pp.) 2000
- [76] Rantalainen, Anna-Lea: Semipermeable membrane devices in monitoring persistent organic pollutants in the environment. (58 pp.) 2000
- [77] Lahtinen, Manu: *In situ* X-ray powder diffraction studies of Pt/C, CuCl/C, and Cu₂O/C catalysts at elevated temperatures in various reaction conditions. (92 pp.) 2000
- [78] Tamminen, Jari: Syntheses, empirical, and theoretical characterization, and metal cation complexation of bile acid-based monomers and open/closed dimers. (54 pp.) 2000
- [79] Vatanen, Virpi: Experimental studies by EPR and theoretical studies by DFT calculations of α amino-9,10-anthraquinone radical anions and cations in solution. (37 pp.) 2000
- [80] Kotilainen, Risto: Chemical changes in wood during heating at 150–260 °C. (57 pp.) 2000
- [81] Nissinen, Maija: X-ray structural studies on weak, non-covalent interactions in supramolecular compounds. (69 pp.) 2001
- [82] Wegelius, Elina: X-ray structural studies on self-assembled hydrogen-bonded networks and metallosupramolecular complexes. (84 pp.) 2001
- [83] Paasivirta, Jaakko (Ed.): CEOEC'2001, Fifth Finnish-Russian Seminar: Chemistry and Ecology of Organo-Element Compounds. (163 pp.) 2001
- [84] Kiljunen, Toni: Theoretical studies on spectroscopy and atomic dynamics in rare gas solids. (56 pp.) 2001
- [85] Du, Jin: Derivatives of dextran: synthesis and applications in oncology. (48 pp.) 2001
- [86] Koivisto, Jari: Structural analysis of selected polychlorinated persistent organic pollutants (POPs) and related compounds. (88 pp.) 2001
- [87] Feng, Zhinan: Alkaline pulping of non-wood feedstocks and characterization of black liquors. (54 pp.) 2001
- [88] Halonen, Markku: Lahon havupuun käyttö sulfaattiprosessin raaka-aineena sekä havupuun lahontorjunta. (90 pp.) 2002
- [89] Falábu, Dezső: Synthesis, conformational analysis, and complexation studies of resorcinarene derivatives. (212 pp.) 2001
- [90] Lehtovuori, Pekka: EMR spectroscopic studies on radicals of ubiquinones Q-n, vitamin K₃, and vitamine E in liquid solution. (40 pp.) 2002

- [91] Perkkalainen, Paula: Polymorphism of sugar alcohols and effect of grinding on thermal behavior on binary sugar alcohol mixtures. (53 pp.) 2002
- [92] Ihalainen, Janne: Spectroscopic studies on light-harvesting complexes of green plants and purple bacteria. (42 pp.) 2002
- [93] Kunttu Henrik, Kiljunen, Toni (Eds.): 4th International Conference on Low Temperature Chemistry. (159 pp.) 2002
- [94] Väisänen, Ari: Development of methods for toxic element analysis in samples with environmental concern by ICP-AES and ETAAS. (54 pp.) 2002
- [95] Luostarinen, Minna: Synthesis and characterisation of novel resorcarene derivatives. (200 pp.) 2002
- [96] Louhelainen, Jarmo: Changes in the chemical composition and physical properties of wood and nonwood black liquors during heating. (68 pp.) 2003
- [97] Lahtinen, Tanja: Concave hydrocarbon cyclophane B-prismands. (65 pp.) 2003
- [98] Laihia, Katri (Ed.): NBC 2003, Symposium on Nuclear, Biological and Chemical Threats – A Crisis Management Challenge. (245 pp.) 2003
- [99] Oasmaa, Anja: Fuel oil quality properties of wood-based pyrolysis liquids. (32 pp.) 2003
- [100] Virtanen, Elina: Syntheses, structural characterisation, and cation/anion recognition properties of nano-sized bile acid-based host molecules and their precursors. (123 pp.) 2003
- [101] Nättinen, Kalle: Synthesis and X-ray structural studies of organic and metallo-organic supramolecular systems. (79 pp.) 2003
- [102] Lampiselkä, Jarkko: Demonstraatio lukion kemian opetuksessa. (285 pp.) 2003
- [103] Kallioinen, Jani: Photoinduced dynamics of Ru(dcbpy)₂(NCS)₂ – in solution and on nanocrystalline titanium dioxide thin films. (47 pp.) 2004
- [104] Valkonen, Arto (Ed.): VII Synthetic Chemistry Meeting and XXVI Finnish NMR Symposium. (103 pp.) 2004
- [105] Vaskonen, Kari: Spectroscopic studies on atoms and small molecules isolated in low temperature rare gas matrices. (65 pp.) 2004
- [106] Lehtovuori, Viivi: Ultrafast light induced dissociation of Ru(dcbpy)(CO)₂I₂ in solution. (49 pp.) 2004
- [107] Saarenketo, Pauli: Structural studies of metal complexing schiff bases, Schiff base derived N-glycosides, and cyclophane π prismands. (95 pp.) 2004
- [108] Paasivirta, Jaakko (Ed.): CEOEC'2004, Sixth Finnish-Russian Seminar: Chemistry and Ecology of Organo-Element Compounds. (147 pp.) 2004
- [109] Suontamo, Tuula: Development of a test method for evaluating the cleaning efficiency of hard-surface cleaning agents. (96 pp.) 2004
- [110] Güneş, Minna: Studies of thiocyanates of silver for nonlinear optics. (48 pp.) 2004
- [111] Ropponen, Jarmo: Aliphatic polyester dendrimers and dendrons. (81 pp.) 2004
- [112] Vu, Mân Thi Hong: Alkaline pulping and the subsequent elemental chlorine-free bleaching of bamboo (*Bambusa procera*). (69 pp.) 2004
- [113]
- [114] Tuononen, Heikki M.: EPR spectroscopic and quantum chemical studies of some inorganic main group radicals. (80 pp.) 2005